A Vector EM System and its Field Applications[1]

by

Gerald W. Hohmann*

Gerald D. VanVoorhis[x]

Philip H. Nelson[+]

*University of Utah

[x]Bear Creek Mining Company

[+]Lawrence Berkeley Laboratory

[1]Presented at the 47th Annual International SEG Meeting, September 20, 1977.

G. W. Hohmann

ABSTRACT

At Kennecott Exploration services we have built and widely applied a unique vector electromagnetic (VEM) system that measures magnetic field amplitude and phase at four frequencies: 26, 77, 232, and 695 Hz. Stable crystal oscillators allow the measurement of phase without a wire link for any transmitter-receiver configuration. A square-wave is transmitted into a loop, and the signal is read at two frequencies; the fundamental and the third harmonic. The amplitude readout is logarithmic with switched 10-decibel gain increments. Amplitude resolution is 0.1 decibel and phase resolution is 0.5 degree.

The VEM system has been applied successfully in a wide variety of exploration terranes and in several field geometries. For reconnaissance work we utilize a large rectangular source loop similar to the Turam geometry, but with only one receiver coil. Amplitude and phase data can be reduced to field strength ratio and phase difference as in Turam or to in-phase and quadrature components. In-phase and quadrature are better for deep targets, because the standard Turam reduction discriminates against deep conductors. For investigating narrow zones or for defining a conductor we use a fixed vertical loop source; in that case the receiver measures the amplitude and phase of the vertical field, rather than the conventional tilt angle. Borehole EM surveys (surface transmitter-downhole receiver and downhole transmitter-surface receiver) are useful both for determining whether an anomaly has been tested by drilling, and for mapping conductors.

G. W. Hohmann

INTRODUCTION

During 1969 and 1970, a versatile set of EM equipment was developed in the electronics laboratory of Kennecott Exploration Services as part of its geophysical research program. The objective of this work was to construct a compact receiver which would precisely measure amplitude and phase over a broad frequency range, with a variety of transmitter-receiver coupling configurations. The objective was achieved by incorporating a pair of stable reference oscillators, one in the transmitter and one in the receiver, in order to provide a synchronous phase reference without a wire link. Phase drifts are small enough, with the particular oscillators used, to permit adequate phase measurement precision for most applications up to one kilohertz. Because the receiver is a vector voltmeter, the equipment is called the Vector EM, or VEM, system. To complete the system we built a transmitter, using a transistor bridge commutator, which can synchronously switch up to 800 watts into a wide variety of loads, including loops and grounded dipoles.

The system is quite versatile; virtually any source-receiver coupling configuration can be used. A variety of field techniques have been developed and used for exploration and research. The widest use for the VEM system has been for Turam surveys with a large fixed rectangular source loop and a single measuring coil. Amplitude and phase data measured by the instrument are easily converted to field-strength-ratio and phase-difference, as in Turam, or to in-phase and quadrature components. In-phase and quadrature component data are better for detection of deep conductors because the standard Turam data reduction discriminates against broad anomalies caused by deep sources and emphasizes narrow anomalies. The system also has been used with a fixed vertical loop source; in that case the receiver measures the amplitude and

phase of the vertical field rather than the tilt angle as measured by conventional gear. This has the advantage of providing a firmer basis for quantitative interpretation than is provided by the tilt angle method.

Another important use of the equipment has been to measure fields in and around exploration drill holes. Both surface source loops with drill hole sensors, and drill hole grounded dipole sources with surface sensors have been used to determine whether a conductor was tested by drilling and whether conductors are continuous.

A crucial part of the VEM program has been the development of interpretation aids, in order to fully utilize the accurate amplitude and phase data for quantitative interpretations. Sophisticated numerical modeling programs were developed at the same time as the instrumentation, and a scale modeling study was carried out for the vertical loop system.

In this paper, we describe the instrumentation and present representative field results. Each field case is accompanied by the appropriate model interpretaton.

G. W. Hohmann

INSTRUMENTATION

The VEM system is comprised of three specially designed components: the receiver, sensing coil, and transmitter, which are described below.

VEM Receiver

Figure 1 is a block diagram of the VEM receiver. The production version has two operating frequencies: 232 and 695 Hz, which are adequate for most uses. When a square wave is transmitted into the source at 232 Hz, a strong third harmonic is generated, and both frequencies can be read at each station without switching the transmitter frequency. For most purposes, we have used an induction coil as the sensing element, but a grounded wire can be used to measure the electric field.

Another version of the receiver measures at two additional frequencies, 26 and 77 Hz, for surveys in conductive areas. The frequency combinations are dictated by the divisions of 5 megahertz which will give the desired fundamental, as well as a counting frequency 720 times the fundamental.

Basically, the receiver consists of a preamplifier, 60-Hz notch filter, two stages of gain-range attenuators and bandpass filters, an amplitude readout, and a phase detector with a reference signal synthesizer driven by a stable crystal oscillator, as shown in Figure 1.

Signal conditioning in the receiver consists of a twin-tee 60-Hz notch filter with 80 db rejection at the fundamental powerline frequency and two Wein bridge bandpass filters connected in series. Each bandpass filter has a Q of 20 and a gain of 100 (40 db). Attenuators, which adjust the signal level in 10 db steps, precede each filter. The maximum gain to the amplitude meter is 100,000 (100 db) and the internal noise level is such that the minimum useful signal is about 10 μv. The filtered and amplified signal goes to an

amplitude measuring circuit and a phase detector. The amplitude signal is rectified and fed to a logarithmic converter which drives a meter calibrated in decibels. By adding the meter reading to the attenuator setting, the signal amplitude is obtained in dB below one volt. The amplitude resolution is 0.1 dB or about 1 percent. Log amplitude values are convenient for computing field strength ratios for Turam applications; only simple differences of adjacent readings are necessary. Tables of normalizing factors in dB have been devised for removing the primary field.

After filtering and gain ranging, the signal goes to a phase measuring circuit where the time difference between its zero crossing and that of a reference signal is measured. The reference signal is generated by a frequency synthesizer, which is driven by a 5 mHz stable oscillator. This oscillator is remarkable in that is has a drift rate of less than 2×10^{-9} parts per 24 hours, and its power consumption is less than one watt. Hence, a maximum relative phase drift of only 0.5 degrees per hour at 100 Hz or 5 degrees per hour at one kHz is specified. In practice the drift rate is less.

A counting frequency 720 times the measurement frequency is generated within the receiver frequency synthesizer, and gated to a counter during the time between zero crossings of the signal and the reference. The counter averages over 100 periods of the signal and displays the results in half-degrees while the next value is being averaged.

For the convenience of the operator, the receiver is split into two units: a frontpack weighing five pounds which contains the measuring instrumentation, and a backpack weighing 13 pounds, which houses the batteries

and power converter. The battery pack consists of 20 D-size rechargeable nickel-cadmium batteries, which will run the receiver for about 8 hours on a full charge.

Sensing Coil

A variety of coils were evaluated in the development program; Figure 2 shows the response function of the induction coil chosen for the production version. It is untuned and is built around a 1/2-in-diameter, 15-in-long, ferrite core. The sensitivity of such a coil in the inductive response region, below the resonance peak, is given by:

$$\frac{V}{H} = A\mu_o K_e n\omega \,,$$

where

V = signal in volts (V)
H = magnetic field in ampere/meter (A/m)
A = area of core in square meters (m^2)
μ_o = free space permeability = 4×10^{-7} henry/meter (H/m)
K_e = effective permeability of core material
n = number of turns
ω = angular frequency

The specified permeability of the core is 4,000, and the effective permeability is about 320 (Keller and Frischknecht, 1966, p. 237). Thirty-thousand turns of wire, wound in two identical sections located symmetrically about the middle of the core, give a sensitivity of 0.95 V/A/m at 100 Hertz. Operating within the linear region of the response curve avoids the tuning and stability problems associated with resonating the coil.

Coil loading strongly affects the resonant frequency and Q of the coil. Figure 3 illustrates the loading arrangement for the production coil. The load consists of an electrostatic shield formed of copper screening and the input impedance of a differential amplifier which is included within the coil package. Electrostatic shielding is important in eliminating capacitive

coupling between the coil windings and the other instrumentation or the operator. It has the same general electrical effect on the coil response as a resistive load; it reduces the Q. Ideally, the shield should be tied to a center-tap between identically wound coil sections.

We have had good results using a high-input-impedance differential amplifier with its ground tied to the coil center tap and shield. This eliminates common mode noise and provides a low-impedance connection to the receiver. The differential amplifier is made up of three integrated-circuit operational amplifiers which have such a low power consumption that even though the unit is continuously energized, the batteries need be changed only at intervals of several months. A loading resistance of one megohm is connected across the coil.

The sensing coil has a resonant frequency of 1600 Hz and is very stable; calibrations at intervals of several months generally repeat within $\pm$ 2 percent. The coil weighs three pounds.

For low-frequency measurements, two ferrite rods are joined end-to-end to form a 30-in-long core, and 100,000 turns are wound in four sections. This gives a sensitivity of 4.8 V/A/m at 100 Hz and a resonant frequency of 450 Hz. A tripod mount is used with this unit for low frequency vertical source loop work.

Transmitter

Power for the transmitter is generated by a 32-volt, three-phase alternator, which is driven by a small gasoline engine. A three-phase transformer with multiple secondary taps is used for impedance matching to the load. The single-phase transformer output is rectified and then commutated by a bridge circuit employing high-voltage transistors. The output voltage is maintained constant by regulating the alternator field winding current. The

commutation circuit is driven by a frequency synthesizer identical to the one in the receiver.

This transmitter will deliver up to 800 watts of power with a peak-to-peak voltage limit of 800 volts and a peak current limitation of four amperes. Normally, the load is tuned using a series capacitance in order to null the load inductance.

SURFACE VEM SURVEYS

We have used the VEM system in two main field configurations for surface surveys: large surface loop (LSL) and fixed vertical loop. In the LSL method, a large, single-turn loop, generally about 2,000 feet on a side, is laid out at the edge of an area to be investigated. Vertical magnetic field measurements are made from the face of the loop out to 2,000 or 3,000 feet along lines about 400 feet apart, and at station spacings of 50 or 100 feet.

The principal advantages of a LSL source are: (1) for a long conductor the depth of exploration is greater than that of dipole source methods; and (2) measurements are not very sensitive to topography. The main disadvantages of the method are: (1) a large area of land control is required for the loop, and (2) the response of a short-strike-length massive sulfide body may be small in comparison to those of longer formational conductors of no economic interest.

A disadvantage with conventional Turam gear is that, in order to obtain phase information, measurements must be made with dual receiver coils. Data are reduced to field strength ratio (FSR) and phase difference ($\Delta\phi$) as follows:

$$FSR = \frac{H_z^n}{H_z^{n+1}} \cdot \frac{H_{zp}^{n+1}}{H_{zp}^{n}} \quad ,$$

and

$$\Delta\phi = \phi_z^n - \phi_z^{n+1} \quad ,$$

where superscripts n and n+1 refer to readings at adjacent stations. H_z and ϕ_z are the amplitude and phase, respectively, of the vertical magnetic field,

and the subscript p refers to the primary magnetic field that would be measured if the earth were not present. Conventional Turam systems, then, measure the magnetic field gradient and discriminate against deep conductors, as we shall subsequently show.

With our VEM gear, we can measure the amplitude and phase of the magnetic field. Thus we are not confined to gradient measurements, although we often reduce the data to FSR and $\Delta\phi$ for simple presentation. Furthermore the VEM gear always provides a measure of anomaly strength, whereas profiles obtained with conventional gear often have gaps over strong anomalies due to limited dynamic range.

For investigating narrow zones we have used a fixed-source vertical loop system. The vertical loop transmitter, with moment ranging from 5500 A-m^2 at 26 Hz to 3500 A-m^2 at 695 Hz, is stationed over a zone to be tested. The field procedure is similar to the conventional fixed transmitter vertical loop method, except that we measure the amplitude and phase of the vertical magnetic field rather than the tilt angle, and hence obtain more diagnostic information. Usually we use a transmitter-receiver profile separation, a, of 400 feet.

For each reading the transmitter loop is rotated so that the receiver is in the plane of the transmitter loop. Thus, if there are no conductors, no signal is received. However, any nearby conductor disturbs the magnetic field, and a signal is measured in this null direction. The amplitude and phase data are reduced to in-phase and quadrature components in mks units, normalized by $m \times 10^{-9}/4\pi$, where m is the dipole moment of the transmitter. System noise (repeatability) is about 5 of these units for a = 400 ft. Interpretation is based on scale model measurements.

The vertical loop method is faster than the LSL method for investigating narrow zones and does not require land control for a large loop. In addition, the vertical loop system is less sensitive to conductor length than LSL, and measurements are more diagnostic of conductivity and depth of burial. However, a serious disadvantage of the fixed-source vertical loop method is that the response decreases rapidly as the transmitter moves away from a conductor. Also, depth of exploration for long conductors is not as great as that of a large-loop system.

Flambeau Ore Body

Figure 4 shows field and theoretical results over the Flambeau ore body, a massive sulfide deposit near Ladysmith, Wisconsin (Schwenk, 1976). Real (R) and imaginary (I) components of the vertical field at 77 Hz, 232 Hz, and 695 Hz are plotted for a traverse over the center of the body. The source was a 1000 x 1400 ft surface loop.

The theoretical model was derived from drill hole information, including resistivity logs and the expected EM response was calculated using the two-dimensional integral equation technique described by Hohmann (1971). Two line sources represent the front and back of the loop. Even though the transmitter loop is small, and the simple model is an approximation to the more complex subsurface, the agreement between field and theoretical results is good. For most LSL interpretation, particularly in conductive terrain, we use a catalog of models computed with the integral equation technique.

Figure 5 shows the same data reduced to FSR and $\Delta\phi$ over 100-foot intervals. Because of the extreme intensity of the anomaly, the Turam scales are much smaller than usual. These data are particularly interesting, because a previous survey with conventional Turam gear failed to provide a measure of anomaly strength due to ranging problems. The dynamic range of the VEM gear

enables us to obtain data over the conductor. In addition, because only a single measuring coil is required, VEM LSL surveys are more efficient than those using conventional Turam dual-coil gear.

Deep Conductors

Conventional Turam reduction acts as a high-pass spatial filter, discriminating against broad anomalies due to deep conductors. In resistive terrain, the in-phase (R) and imaginary (I) components of the vertical magnetic field provide greater depth of exploration.

The advantage of magnetic field measurements over gradient measurements is illustrated in Figures 6 and 7, which show FSR- $\Delta\phi$ and R-I data, respectively at 232 Hz over a deep conductor in Minnesota. The conductor is a narrow massive sulfide body more than 300 ft deep. Overburden is very thin, and the host rock is highly resistive. We used a 2000 x 2000-foot source loop and took readings at 100-foot station spacings on a grid. Data for four of the grid lines are shown in Figures 6 and 7. There are no significant anomalies in the FSR- $\Delta\phi$ data of Figure 6; on the other hand there is a clear anomaly in the R-I data of Figure 7.

To interpret these data we use the two-dimensional numerical model results shown in Figures 8 and 9 for FSR- $\Delta\phi$ and R-I, respectively. The theoretical results, taken from a model catalog, are shown for vertical and horizontal slabs, each 400 feet deep. The similarity between the theoretical curves and the field data of Figures 6 and 7 is striking. It appears that a deep conductor is present below station 14 on each of the lines. The theoretical FSR- $\Delta\phi$ results of Figure 8 explain the absence of a notable anomaly in the Figure 6 field data; the gradient reduction has filtered out the long-wavelength anomaly due to the deep conductor. The theoretical results also illustrate that for a deep conductor it is impossible to

distinguish between vertical and horizontal orientation.

Figure 10 shows vertical loop data over a deep conductor in Western Australia in an area of high overburden resistivity. In-phase and quadrature components of the vertical magnetic field are shown for frequencies 77, 232, and 695 Hz. The separation, a, between the receiver line and the transmitter was 400 ft. The massive sulfide body is about 200 ft deep and 25 ft thick, based on drilling results. Its width decreases rapidly along strike in either direction, the massive sulfides grading into disseminated pyrrhotite, which does not produce an EM anomaly. Hence this short-strike-length conductor may not be a good LSL target.

The vertical loop data show a good anomaly. Interpretation based on scale model results yields a conductivity-thickness (σt) of 40 mhos, indicating that the bulk resistivity is about 0.2 ohm-m. The EM depth estimate is 170 ft, which is in good agreement with the reported depth of 200 ft.

Conductive Environment

The major types of noise in EM surveys are: (1) geologic noise (overburden conductors, graphite), (2) system noise (electronic noise, coil orientation errors), (3) cultural noise (powerlines, fences, pipelines), and (4) disturbance field noise (sferics, powerlines). In conductive terrain such as Western Australia, the most important type is geologic noise, which arises from lateral variations in the low-resistivity overburden. Differential weathering and permeable shear zones are important causes of lateral variations. Sources of geologic noise in the overburden generally are not as conductive as massive sulfides, but they are shallow, and thus may produce anomalies that are comparable to or greater than anomalies due to good conductors in the bedrock.

Some means must be used to discriminate among the numerous EM anomalies that arise in surveys where overburden is thick and conductive. The two common means of discrimination are: (1) correlating with other types of information, and (2) selecting only good conductors. In the first method, EM anomalies that have associated magnetic, gravity, geochemical, or IP anomalies, e.g., are selected for further investigation. Hence, this method applies more to detailed investigations where other types of information are available, than to reconnaissance surveys. The second method requires that targets of interest be better conductors than sources in the overburden. Then, by using low frequencies, by measuring amplitude and phase, and by choosing the optimum coil configuration for a particular target, one can achieve some success in determining which anomalies are due to good conductors in the bedrock.

Theoretical Results: The principle is illustrated in Figures 11 and 12, which show two-dimensional numerical model results for the Turam method. Two line sources, 2000 feet apart, represent the source loop. The curves in Figure 11 are for an overburden conductor, while those in Figure 12 pertain to a good conductor in bedrock beneath conductive overburden. Results are shown for four frequencies: 26, 77, 232, 695 Hz. The response of the overburden conductor diminishes rapidly as the frequency decreases, while that of the bedrock conductor decreases less rapidly and is large even at 26 Hz. Hence a multifrequency EM system provides better detection and resolution of good conductors through both a knowledge of frequency response and an increase in target response compared to geologic noise at the lower frequencies.

Field Data-Geologic Noise: Four-frequency LSL data from a deeply weathered nickel prospect in western Australia are shown in Figure 13. An aeromagnetic survey and trenching defined a prospective ultramafic body between 2W and

9.5W. Resistivities (from an IP survey) are as low as 5 ohm-m and highly variable due to differential weathering. The water table is about 200 ft deep. The basal contact of the ultramafic was drilled and intersected on this line at 9.5W and at several other locations along strike. No mineralization was encountered.

Geologic noise is very high in the EM data due to the deep differential weathering. However, the geologic noise is much less at the lower frequencies, so that it would be possible to detect a conductor with a good response at low frequencies, provided it were not too deep. Low-resistivity overburden such as this is prevalent over much of Western Australia; in some cases overburden resistivity is less than one ohm-meter, which precludes EM work.

Figure 13 illustrates an unfortunate problem for nickel exploration in Western Australia. Magmatic differentiation deposits occur at the basal contact of an ultramafic body, but often there is, as at station 9.5W in this case, a strong anomaly due to a shallow conductor along the entire contact. An IP line run to investigate this anomaly confirmed that the EM response is not due to sulfides, but rather to a permeable (shear?) zone. Detection of a small nickel deposit at depth beneath this shallow conductor would be quite difficult with EM.

To investigate the shallow conductor further, we ran several vertical loop profiles over the contact. Typical data are shown in Figure 14 for the same line as Figure 13. Because the vertical loop energizes only a narrow zone, it provides more diagnostic information for a particular conductor in this environment. Interpretation using scale model results suggests that the EM anomaly is due to a 10- to 15- mho overburden conductor. More realistic model curves based on a conductor in a conductive half space probably would

produce a slightly different interpretation. Because the vertical loop response of the overburden conductor is small at 26 and 77 Hz, we might expect to detect a very good conductor at depth, if one were present.

Field Data-Massive Sulfide: Figure 15 shows four-frequency LSL data over the Freddie Well deposit, a shallow massive sulfide body in Western Australia, at a location where overburden conditions are more favorable for EM. Massive and disseminated mineralization occurs over a 100-ft interval centered at 0 on the line. Its electrical conductivity is high due to well-connected pyrite and pyrrhotite lenses. Background resistivity ranges between 30 ohm-meters on the west end of the line and 300 ohm-meters to the east.

The large responses at 26 Hz and 77 Hz show that the anomaly is due to a very good conductor - the type that could be detected even through the geologic noise of Figure 13. Numerical modeling suggests that the bulk resistivity of the body is 0.1 to 0.3 ohm-m, and its depth is about 100 ft.

Vertical loop results for the same line are shown in Figure 16. Again, the anomaly is large at all frequencies. Interpretation based on free-space, thin-conductor scale models yields σt estimates of 500, 200, 70, and 25 mhos at 26, 77, 232, and 695 Hz, respectively. Thus, the scale model results for a thin sheet are not applicable. We also attempted to interpret the Turam data using Lamontagne's (1970) free-space and numerical models: only the 26 Hz and 77 Hz data resemble the model results closely enough to permit parameter estimation, yielding σt estimates of 700 and 150 mhos, respectively. Hence numerical modeling is necessary to interpret EM anomalies over this conductor in order to account for its width and for the host rock resistivity.

Mayr's formula (Lamontagne, 1970) for the critical thickness, t_c, at which a body no longer behaves as a thin conductor for Turam interpretation is

$$t_c = 300 \quad (\rho / f)^{\frac{1}{2}}$$

Hence, for ρ = 0.3 ohm-meters we have t_c =32, 19, 11, 6 meters at 26, 77, 232, and 695 Hz, respectively. For ρ = 0.1 ohm-meters, the corresponding t_c values are: 19, 11, 6, and 4 meters. Because this conductor is about 30 meters thick, and numerical modeling indicates that its resistivity is between 0.1 and 0.3 ohm-meters, it behaves as a "thick" conductor at all frequencies.

The vertical loop method is quite selective of conductors near the transmitter loop, as Figure 17 dramatically illustrates. It shows vertical loop data for the same line as Figure 16, but with the transmitter 400 feet off the axis of the conductor. The anomaly is negligible. This aspect of the fixed-source vertical loop method makes it useful for selectively energizing a narrow zone, but renders it unsuitable for reconnaissance work.

Figures 18 and 19 show LSL and vertical loop data, respectively, over the "D" shoot at the Mount Windarra nickel deposit in Western Australia. The EM response is dominated by a thick section of sulfide facies banded iron formation (BIF), which begins about 100 feet from the nickel orebody. Evidently, the orebody is not a good conductor, for it produces only a small response at 77 Hz and none at 26 Hz. The orebody response appears as a small FSR peak with the LSL method and as a cross-over with the vertical loop technique. Due to the iron formation response, the vertical loop peak on the left side of the cross-over is larger than that on the right side. Interpretation of the anomaly due to the nickel ore body is difficult due to

interference from the banded iron formation. Farther along strike, there is no separate EM response over the "A" shoot (not shown), because it is only 50 feet from the iron formation. Hence EM exploration is very difficult in the Mt. Windarra environment.

G. W. Hohmann

DRILL HOLE EM SURVEYS

There are numerous reasons for conducting drill hole EM surveys: checking the adequacy of a drilling program, exploring for an extension of a known deposit, and examining the electromagnetic character of a known deposit to aid the design of future exploration programs. The field cases described in this section were conducted for combinations of these reasons. We employed surface sources and downhole coil receivers in most instances, but we have also used downhole electrode excitation in conjunction with surface measurements. In all cases the equipment is as described above, but with the downhole coil suitably simplified and encapsulated to permit operation in a water-filled NX-size borehole. In many field situations it would be desirable to obtain information between boreholes; for this purpose both the receiver and transmitter would be located in boreholes. We did not work with the cross-hole configuration, but the VEM system is quite adaptable to that kind of use.

Determination of Drill Hole Intercept

In many cases it is not clear whether or not drilling has adequately tested an electromagnetic anomaly observed on the surface. The drill may have penetrated too high or too low, in which case electromagnetic logging may help to determine the position of the conductor. Or in the case of poor conductors, the core may contain only marginal evidence of electrically conductive material; borehole measurements can determine if the conductor was penetrated.

First example. Figure 20 shows the plan map and cross section of drill hole SC-2, originally drilled to test an airborne EM anomaly. The test was made to determine if the zone of pyrrhotite caused the surface anomaly or if additional drilling was warranted. Measurements were obtained downhole at

five-foot spacings and on a north-south surface line at 50-foot spacings over SC-2, first using the north loop, then the south loop as a transmitting source. The downhole EM results are shown in Figure 21 along with magnetic susceptibility measurements made on core. Each susceptibility data point is an average over six feet of core, with three to four measurements per foot where the susceptibility changed rapidly.

Interesting features of the data are:

1. The total amplitude increases down the hole with the transmitter at 1,000 S and decreases down the hole with the transmitter at 1,000 N. In both cases, the field decreases as the coil moves from the source side of the conductor to the "shadow" side. This behavior is in agreement with model results and with our intuitive expectations.
2. A small bump in the amplitude at 245 feet is due to a 2-foot band of magnetite. The phase is not affected, as we expect for a permeable, non-conductive body. Notice how small the amplitude change is, even though the coil is within the permeable material.
3. Both phase traces undergo rapid changes at 150 and 190 feet. This is the behavior we expect to observe in passing through a conductor, so we can assume that current axes exist at approximately these depths. The conductor axis at 150 feet shows up nicely as a peak in the susceptibility log, so we have good evidence that the pyrrhotite is the conductor, although the correlation at 190 feet is not quite as good.

Figure 22 is a composite of the field data and a two-dimensional model computed by the network analogy technique (Swift, 1971). The numerical model has two parallel conductors of 2 ohm-meters which are each 10 feet thick and 20 feet apart beneath 50 feet of overburden. Superimposed on the phase contours of the theoretical model are the phase data with the source on the

left-hand side. The match between the field data and the model is quite good both qualitatively and quantitatively, and could be improved just by manipulating slightly the relative position of the drill hole with respect to the model. The correspondence of the field and theoretical amplitudes also is good, but the phase is more definitive.

Notice that the model predicts smooth phase behavior on the source side of the conductors, while fairly strong changes occur on the shadow side. The field data behave similarly. If a test hole had been drilled parallel to, but had missed the conductor, this phenomenon would provide us with directional information on the conductor location, assuming a test similar to this one could be carried out.

Second example. Figure 23 shows the plan and cross section at a location where two holes were drilled, both failing to intercept a significant conductor. Downhole VEM data were obtained in both holes; the 232-Hz amplitude results are shown in Figure 24 for the two large-loop sources. The logs from SI-1 show no significant attenuation which would result from penetrating a conductor. The amplitude increases at 185 ft are accounted for if the top of the conductor lies just below the drill hole, which seems plausible in terms of the geometry and the reported depth of oxidation (see cross section in Figure 23). The amplitude level is constant with depth in SI-1 for north loop excitation because the hole angle causes the coil to approach the loop as the depth increases. Similarly, the amplitude level in SI-1 decreases with depth for south loop excitation, due to the geometry and attenuation of the field in the earth.

The logs from SI-2 show fluctuations at 440 ft and at 490 ft. For the north loop the amplitude drops as the coil passes from the source side to the shadow side of the conductor. Similarly, with south loop excitation the

amplitude increases in passing from the shadow side to the source side. The two conductors detected by the logs are indicated in the cross section of Figure 23.

The core recovered from SI-1 contained only weak disseminated sulfide mineralization, less than 1 percent pyrrhotite and pyrite, from 146 to 176 feet (Fig. 23). The EM amplitude peak at 185 feet is obviously associated with this small amount of sulfides. In SI-2 both EM anomalies occur where sulfides are present (predominantly pyrrhotite) at the level of several weight percent. Despite the low levels of sulfides, the drill hole measurements leave no doubt that the plane of the conductor detected at surface has been tested, although it appears that more massive material exists between the two drill hole intersections. Due to lack of encouragement in the core for economic mineralization, no further drilling was done.

Field Study of a Flat-Lying Ore Deposit

Figure 25 shows the locations of four drill holes and the depth of the sulfides below the surface at Kennecott's Arctic massive sulfide deposit in Alaska. The deposit was discovered on a geochemical-geological reconnaissance: it outcrops to the east. The deposit is roughly pancake-shaped, with a shallow dip relative to the topography. The EM test was undertaken to see if the main part of the deposit could be detected at the surface despite depths in excess of 300 ft. A secondary purpose was to determine with drill hole measurements whether or not non-economic conductors were present.

A large loop about four miles in circumference was laid out around the deposit and driven with a two-ampere current. Eleven drill holes were logged and about 6 miles of line were read at 232 Hz and 695 Hz. The limited area of Figure 25 is discussed here because it demonstrates all of the important

results. Because 695-Hz measurements show a greater response than do 232-Hz measurements, only the 695-Hz data are presented.

The disk model in Figure 26 displays the theoretical secondary fields produced by currents induced by a uniform primary field (Greenfield, 1971). The dip of the disk and the uniform primary field are reasonable for our field case, but we cannot expect to duplicate exactly the drill hole results due to heterogeneity of the conductor, departure from the disk geometry, finite host rock conductivity, etc. Nevertheless, the results from a line of four drill holes across the deposit boundary (Fig. 27) definitely resemble the response of the disk model. The field data show a greater response than the model results and display erratic detail, since the deposit is not at all a single homogeneous unit. Also, DDH-9 is sufficiently removed from the edge of the deposit that no inflections occur.

Prior to the drill hole surveys, we suspected that graphite was present in amounts sufficient to behave as a conductor. The surveys showed that this was not the case; in all the holes surveyed, EM anomalies occurred only where sulfides are present. Hence, the surface survey anomalies are caused only by the massive sulfide mineralization.

Figure 28 displays the calculated surface response for the disk model. The asymmetry of the signature results from the proximity of the surface to the upper edge of the dipping disk and the tendency of the induced currents within the disk to crowd toward the perimeter. Note that the FSR and $\Delta\phi$ anomalies lie very nearly above the outer edge of the disk. Figure 29 displays the amplitude ratios and phase differences computed from the field measurements (within the source loop) for the east-west lines, and shows the anomaly locations for the north-south lines as well as the east-west lines. The anomalies are roughly the same magnitude for both directions of survey

traverses, and the combined results from the two survey directions trace an arcuate boundary which, according to the model results, corresponds to the boundary of the conductor.

Downhole Source and Surface Receiver

At another site we addressed the problem of mapping long sinuous conductors lying at 300-ft depths. Drilling showed that the massive sulfides occurred in the shape of undulating shoestrings, about 1,200 ft long, 100-200 ft wide and 20-45 ft thick. It was possible to map them using a surface source and surface receiver, but existing drill holes afforded an opportunity to use a downhole source and map more accurately than would be possible with surface methods alone.

A fundamental problem in most EM techniques is to account for the primary field. Some systems incorporate compensation circuitry in the electronics (slingram), others normalize to the primary field in the computation process (Turam), and some measure in the null field of the primary (vertical loop). We have presented examples of the latter two techniques in the preceding section on surface surveys. Another approach is to minimize the primary field by removing it as far as possible from the receiver while maximizing the source-target coupling. This is the reason for putting the EM source down a drill hole.

In our experiment we attached an electrode to the cable end and a second one about 200 feet above the end. Both were made of plumber's "lead wool" surrounded by salt-impregnated foam rubber, and taped to the cable. The electrodes were about 10 feet in length. The cable was lowered down the hole until the upper electrode was in the vicinity of the conductive zone. The resistance between electrodes was then monitored while the cable was raised or lowered to find the minimum resistance. This assured that the conductor was

between the electrodes. The EM transmitter drove the electrode pair from the surface.

With the current return below the top of the conductor, the resultant "transmitting antenna" comprised of the electrodes and the conductor appears to function as a pair of vertical loops. That is, the vertical field due to the conductor will be null and will undergo a 180-degree phase change directly above the conductor, while the horizontal field will be maximum at the same point. In fact, the result should be like that pictured in Figure 16.

Figures 30 and 31 exhibit vertical field data over the grid for transmitters in two different drill holes. The amplitude data are plotted on a logarithmic scale as read from the receiver, rather than as in-phase and quadrature components. The signal levels were quite low. The 180-degree phase change is located by an arrow and the symbol "$\Delta\phi$". In general, it coincides with the amplitude null.

The clearest results are shown in Figure 30 for DH 77 (see Fig. 32 for the positions of the drill holes and the anomalies). It is interesting that DH 77 did not intersect the conductor according to core logging. Yet drill hole EM logging (not shown) showed that the hole was very close to a conductor at 380 ft so the upper electrode was placed there. The transmitter has clearly energized a conductor with a strike length of 1,800 ft, as indicated in Figure 30. Continuity along strike is implied.

Figure 31 contains similar results for downhole excitation in DH 72. Another conductor with east-west strike is traced for 1,400 feet. Figure 32 shows the trace of this conductor at the north edge of an anomaly mapped with the surface loop and surface receiver. The anomaly shows good continuity and is a worthwhile drill target. Other less definitive anomalies appear on

the western portion of the grid. Their trace is not indicated in the summary of Figure 32.

CONCLUSION

The VEM system is reliable, easy to use, and versatile. It provides accurate, multi-frequency, amplitude and phase data for any transmitter-receiver configuration without a wire link. We have used it successfully for both surface and drill hole surveys. Sophisticated interpretation aids are required to take advantage of the diagnostic information provided.

Better electronic components have become available since the VEM system was designed, so that the weight and size could be reduced and the accuracy could be improved. Any redesign should utilize coherent detection for greater noise rejection.

ACKNOWLEDGMENTS

A number of Kennecott geophysicists and technicians helped develop and deploy the VEM gear. Especially important were initial conversations with Charles Swift, and the engineering help provided by Dale Green. The first routine applications were carried out by Carl Schwenk and Clark Topping. We thank Kennecott Copper Corporation for permission to publish this paper, Western Mining Corporation for permission to publish the Mt. Windarra data, and C. R. A. Exploration for permission to publish the Freddie Well data.

FIGURE CAPTIONS

Figure 1. Block diagram of the Vector EM (VEM) Receiver.

2. Induction coil response.

3. Loading arrangement for induction coil.

4. Field and theoretical large-loop results over the Flambeau ore body, Wisconsin.

5. Flambeau data of Figure 4 reduced to Turam format.

6. LSL data over a deep conductor in Minnesota.

7. Real and Imaginary components for same survey as that shown in Figure 6.

8. Theoretical FSR-$\Delta\phi$ results for deep conductors.

9. Theoretical real and imaginary results used to interpret the data in Figure 7.

10. Vertical loop data over a deep conductor in Western Australia.

11. Theoretical FSR-$\Delta\phi$ results for an overburden conductor.

12. Theoretical FSR-$\Delta\phi$ results for a good conductor in bedrock.

13. LSL data from a deeply weathered nickel prospect in Western Australia.

14. Vertical loop data for the same line as that shown in Figure 13.

15. LSL data over the Freddie Well massive sulfide deposit in Western Australia.

16. Vertical loop data for the same line as that shown in Figure 15.

17. Vertical loop data for the same line as Figure 15, but with the transmitter 400 feet off the axis of the conductor.

18. LSL data over the Mt. Windarra nickel deposit, Western Australia.

19. Vertical loop data at Mt. Windarra, Western Australia. Same line as Figure 18.

20. Plan map and cross-section for drill hole SC-2.

21. Downhole EM log and core magnetic susceptibility in drill hole SC-2.

22. Contours of constant phase (degrees) from numerical model with the phase data from SC-2 superimposed.

23. Plan map of drill hole collars and source loops (upper) and cross-section of drill hole location (lower) with interpreted results.

24. Downhole EM amplitude logs at 232 Hz in SI-1 and SI-2.

25. Depth (feet) of sulfides below surface. Arctic, Alaska massive sulfide deposit.

26. Computed "drill hole" response of a dipping circular disk in a uniform vertical field. Location is scaled in units of one disk radius.

27. VEM logs at 695 Hz of four drill holes in Arctic deposit, referenced to free space primary field.

28. Computed in-phase (R), quadrature (I), reduced ratio (FSR), and phase difference ($\Delta\phi$) over a dipping 3-mho disk in a uniform vertical field. Survey line is 0.5 disk radius above center of disk.

29. VEM FSR and $\Delta\phi$ data at 695 Hz plotted on plan map of survey area. Horizontal bars denote anomaly locations determined from the east-west data; similar data on north-south survey lines produced the vertical bars.

30. Amplitude (decibels) of vertical field component at 232 Hz, with downhole electrode source in DH 77. The arrows below the $\Delta\phi$ symbols denote the location of 180° phase changes. Line and station numbers designate hundreds of feet. Drill hole 77 is located at 20.3N, 9.7W on the grid. The downhole source in drill hole 77 is an upper electrode at 390 feet, lower electrode at 590 feet.

31. Downhole source at 370-570 feet in drill hole 72 located at 14.2N, 21.4W on the grid.

32. Results of VEM surface measurements on grid using both down-hole and surface sources. Grid coordinates given in hundreds of feet.

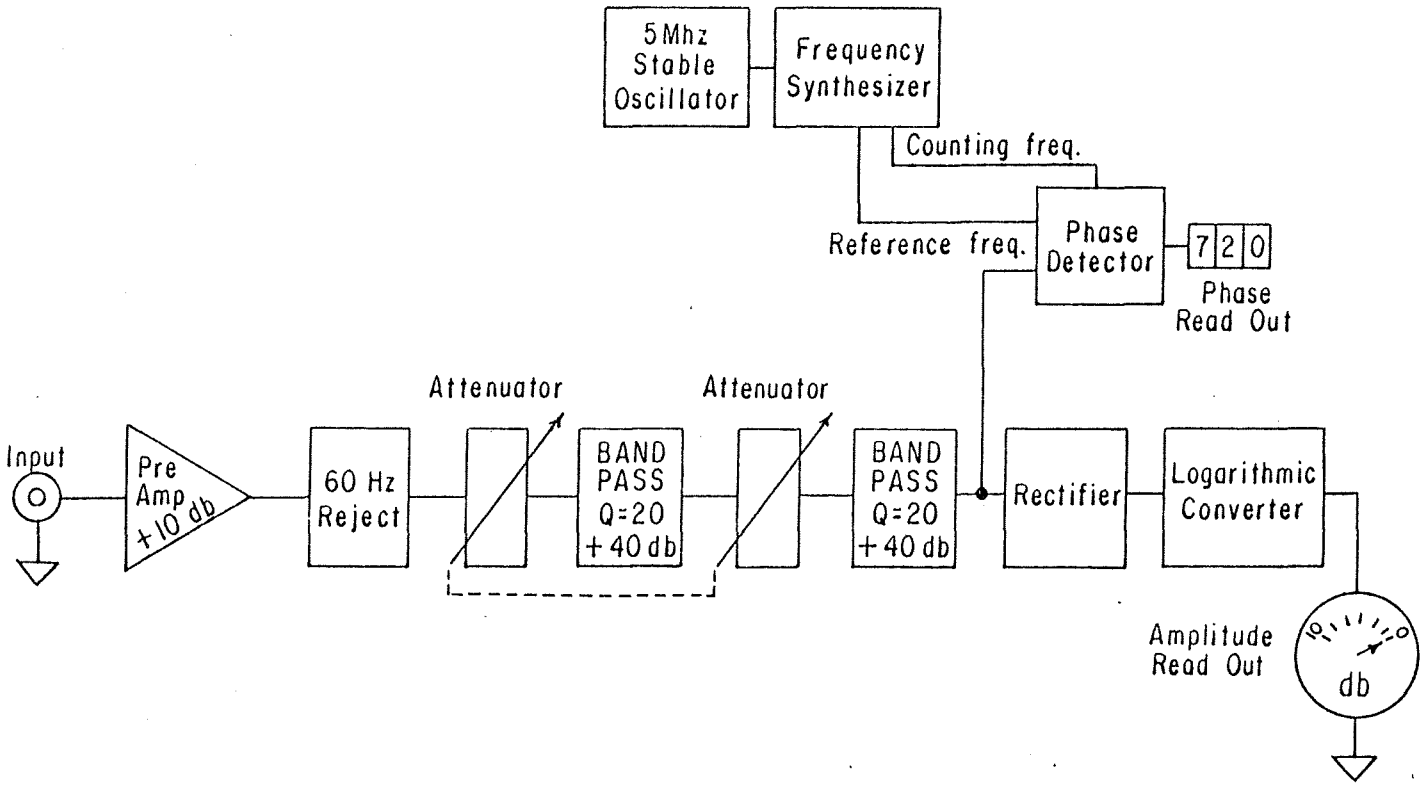
5 Mhz Stable Oscillator
Frequency Synthesizer
Counting freq.
Reference freq.
Phase Detector
7 2 0
Phase Read Out
Attenuator
Attenuator
Input
Pre Amp +10 db
60 Hz Reject
BAND PASS Q=20 +40 db
BAND PASS Q=20 +40 db
Rectifier
Logarithmic Converter
Amplitude Read Out
db

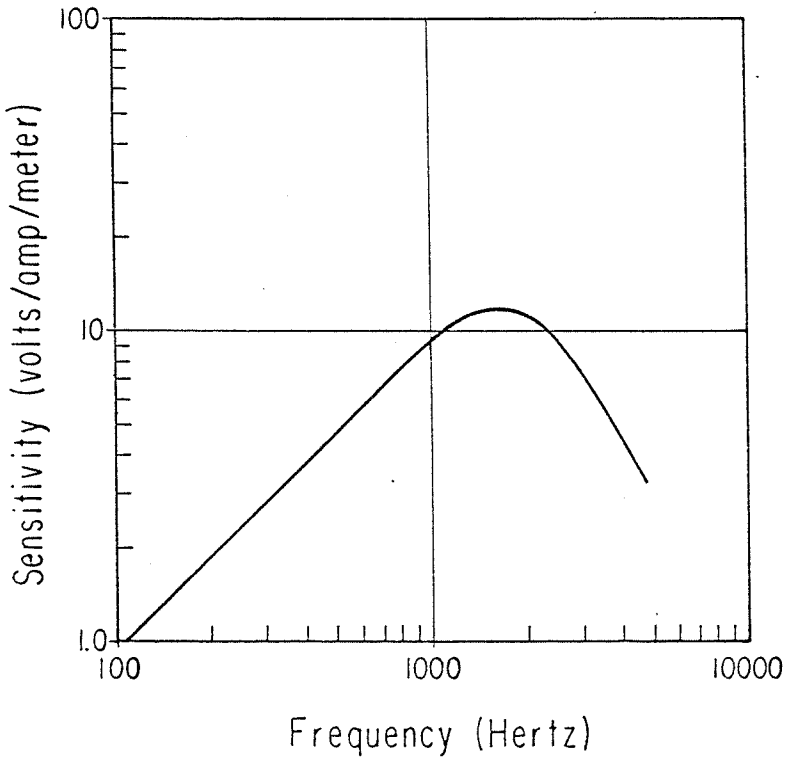
100
10
1.0
Sensitivity (volts/amp/meter)
100
1000
10000
Frequency (Hertz)

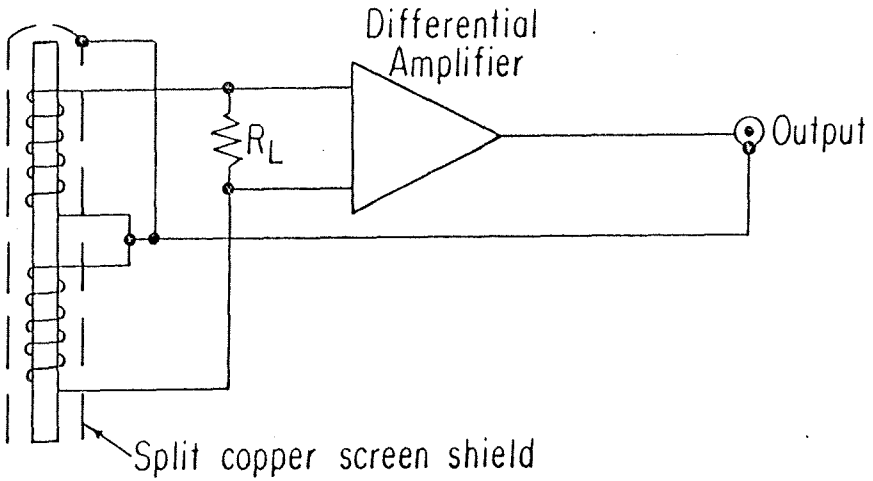
Differential
Amplifier
R_L
Output
Split copper screen shield

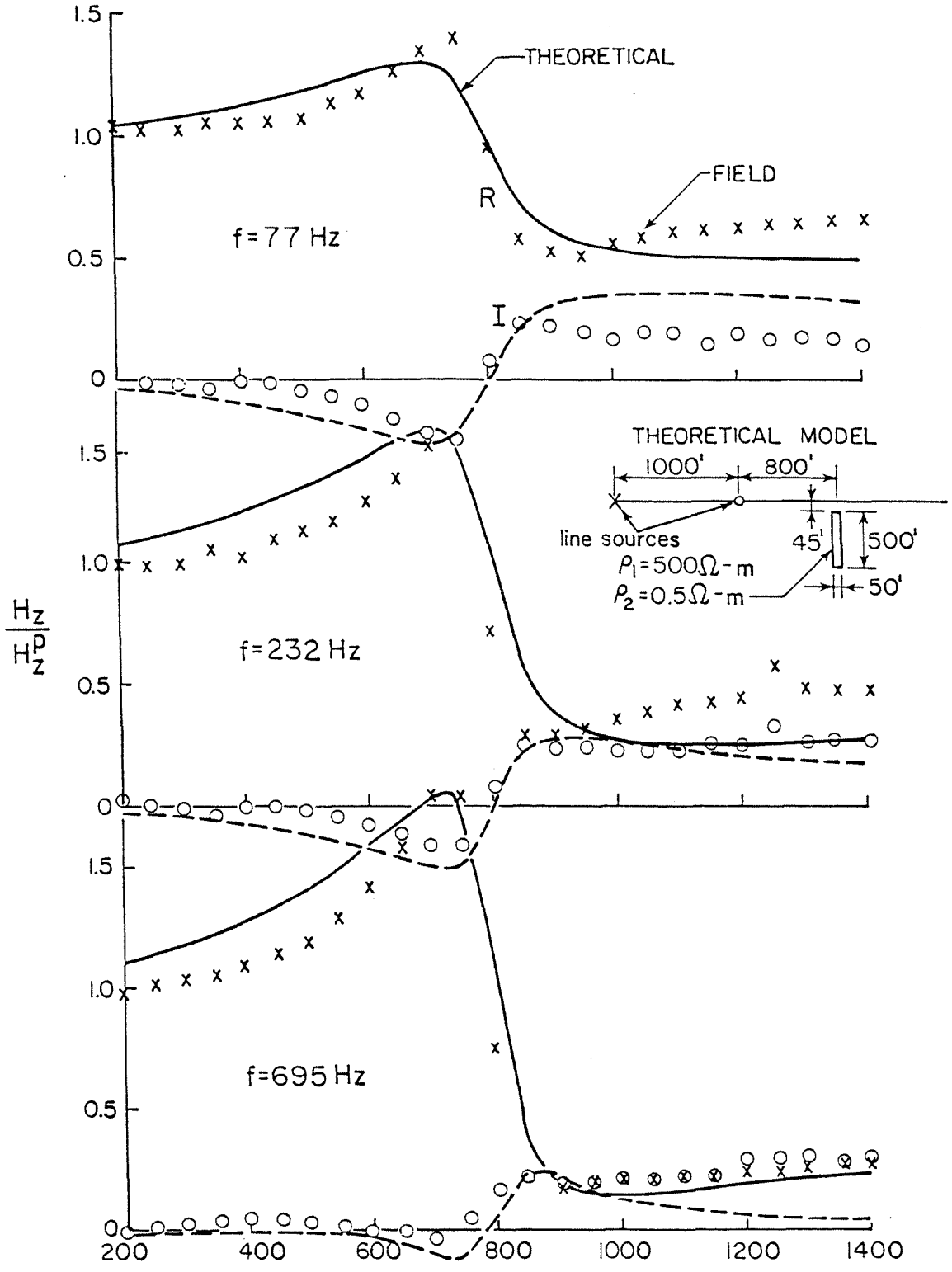
THEORETICAL
FIELD
R
I
f=77 Hz
f=232 Hz
f=695 Hz
THEORETICAL MODEL
1000'
800'
line sources
45'
500'
ρ_1=500Ω-m
ρ_2=0.5Ω-m
50'
$\frac{H_z}{H_z^p}$
1.5
1.0
0.5
0
200
400
600
800
1000
1200
1400

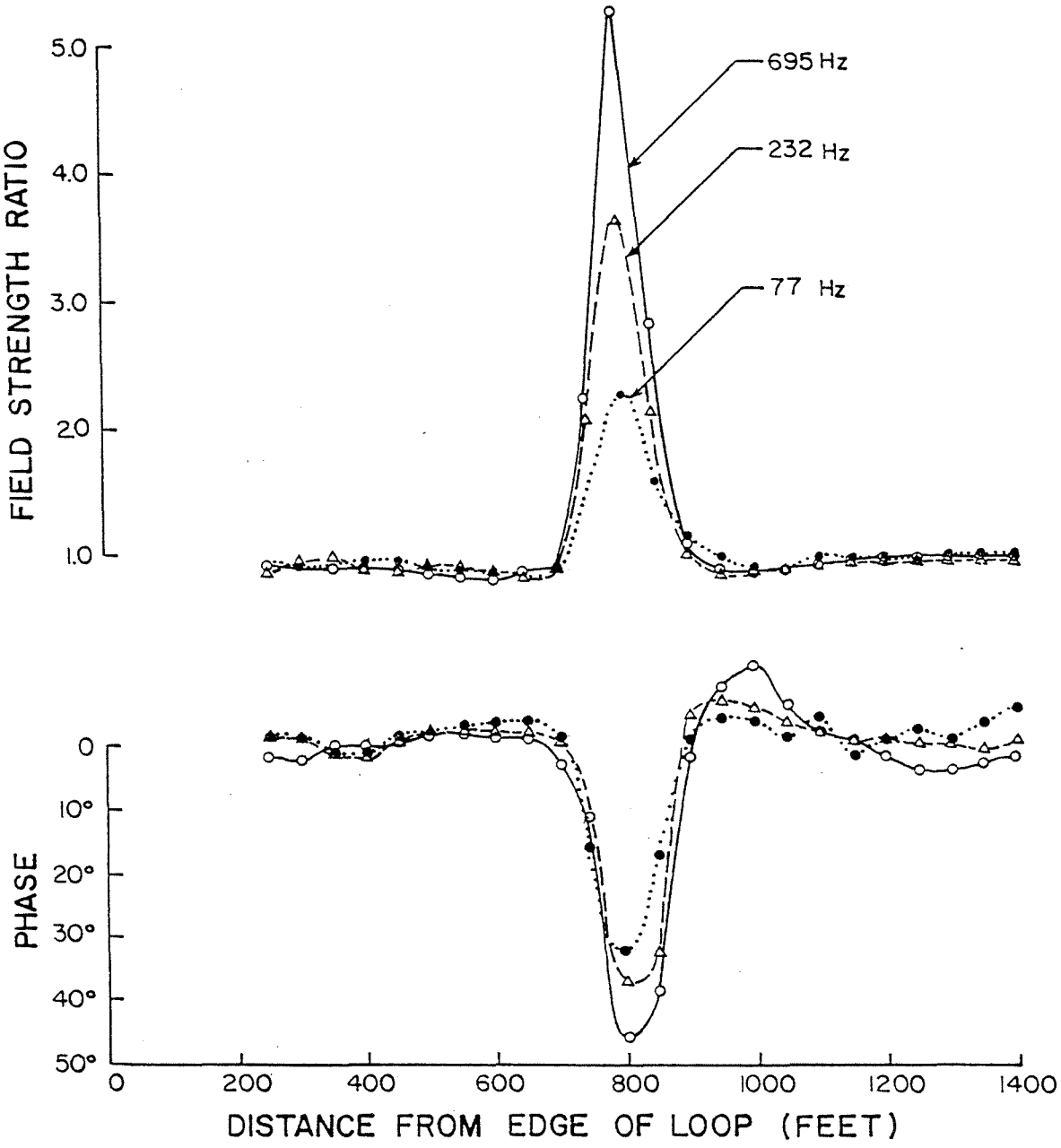
FIELD STRENGTH RATIO
5.0
4.0
3.0
2.0
1.0
695 Hz
232 Hz
77 Hz
PHASE
0
10°
20°
30°
40°
50°
0
200
400
600
800
1000
1200
1400
DISTANCE FROM EDGE OF LOOP (FEET)

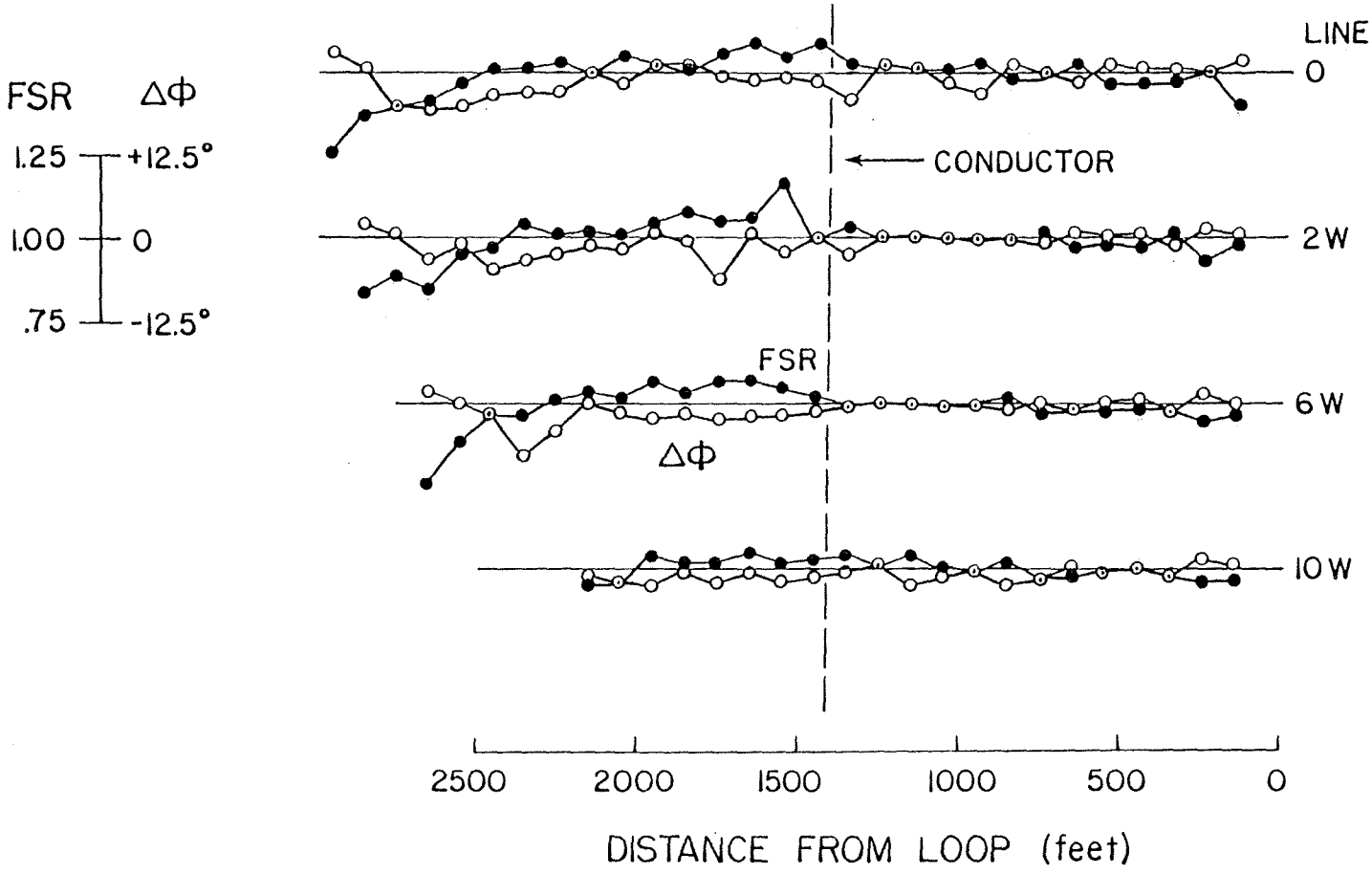
FSR
ΔΦ
1.25
+12.5°
1.00
0
.75
-12.5°
LINE
0
CONDUCTOR
2W
FSR
6W
ΔΦ
10W
2500
2000
1500
1000
500
0
DISTANCE FROM LOOP (feet)

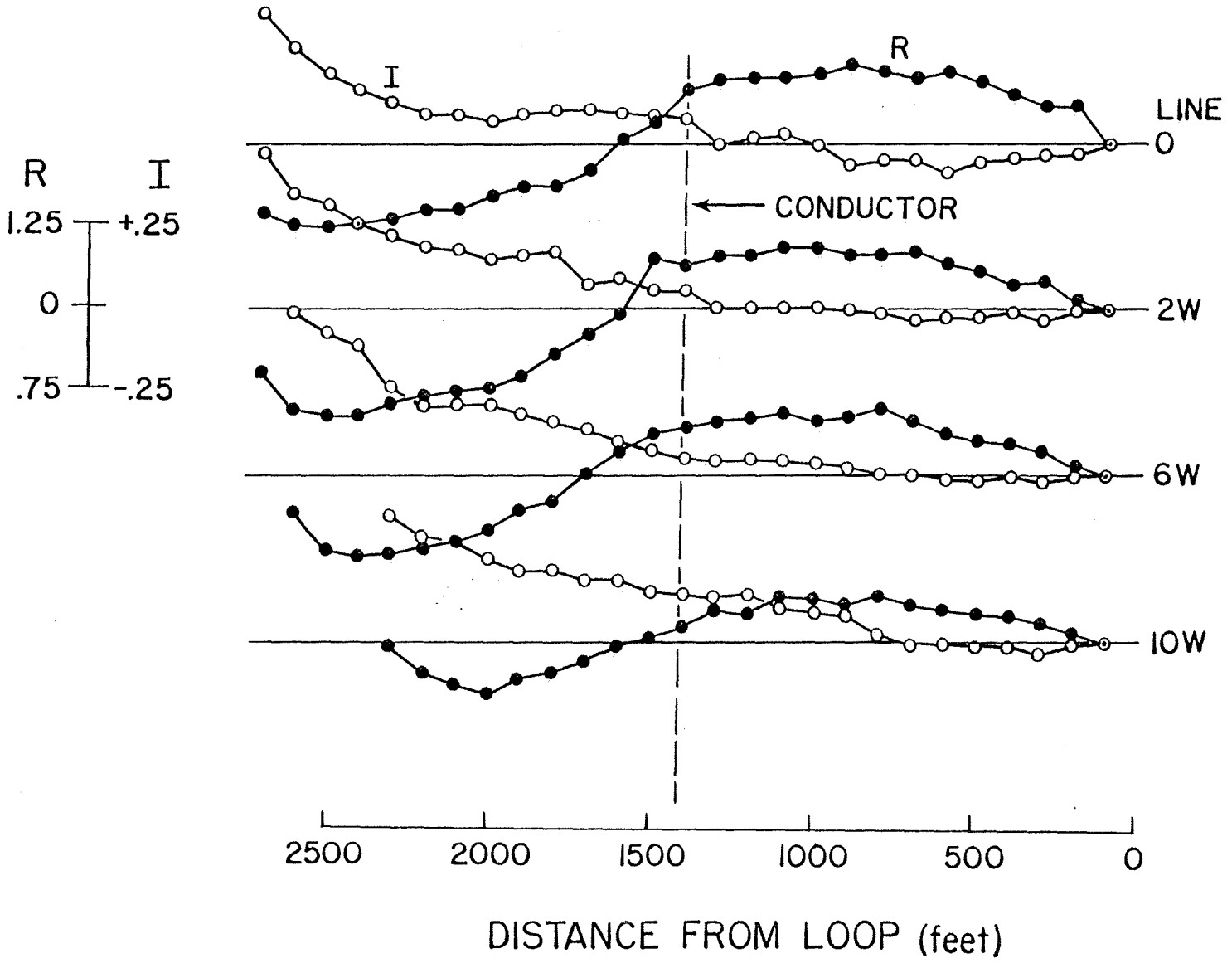
R
I
1.25
+.25
0
.75
-.25
I
R
LINE
0
CONDUCTOR
2W
6W
10W
2500
2000
1500
1000
500
0
DISTANCE FROM LOOP (feet)

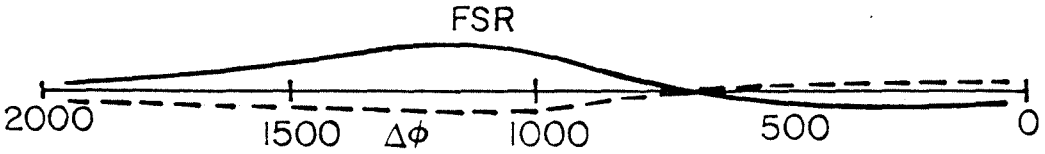
FSR
2000
1500
Δφ
1000
500
0

500 Ω-m

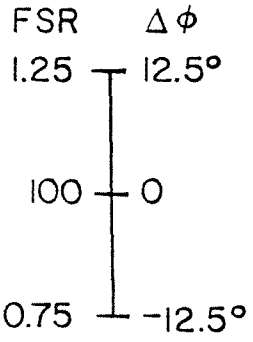
FSR
Δφ
1.25
12.5°
100
0
0.75
-12.5°

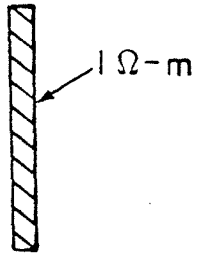
1 Ω-m

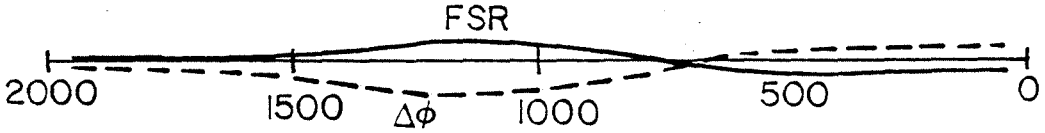
FSR
2000
1500
Δφ
1000
500
0


5Ω-m

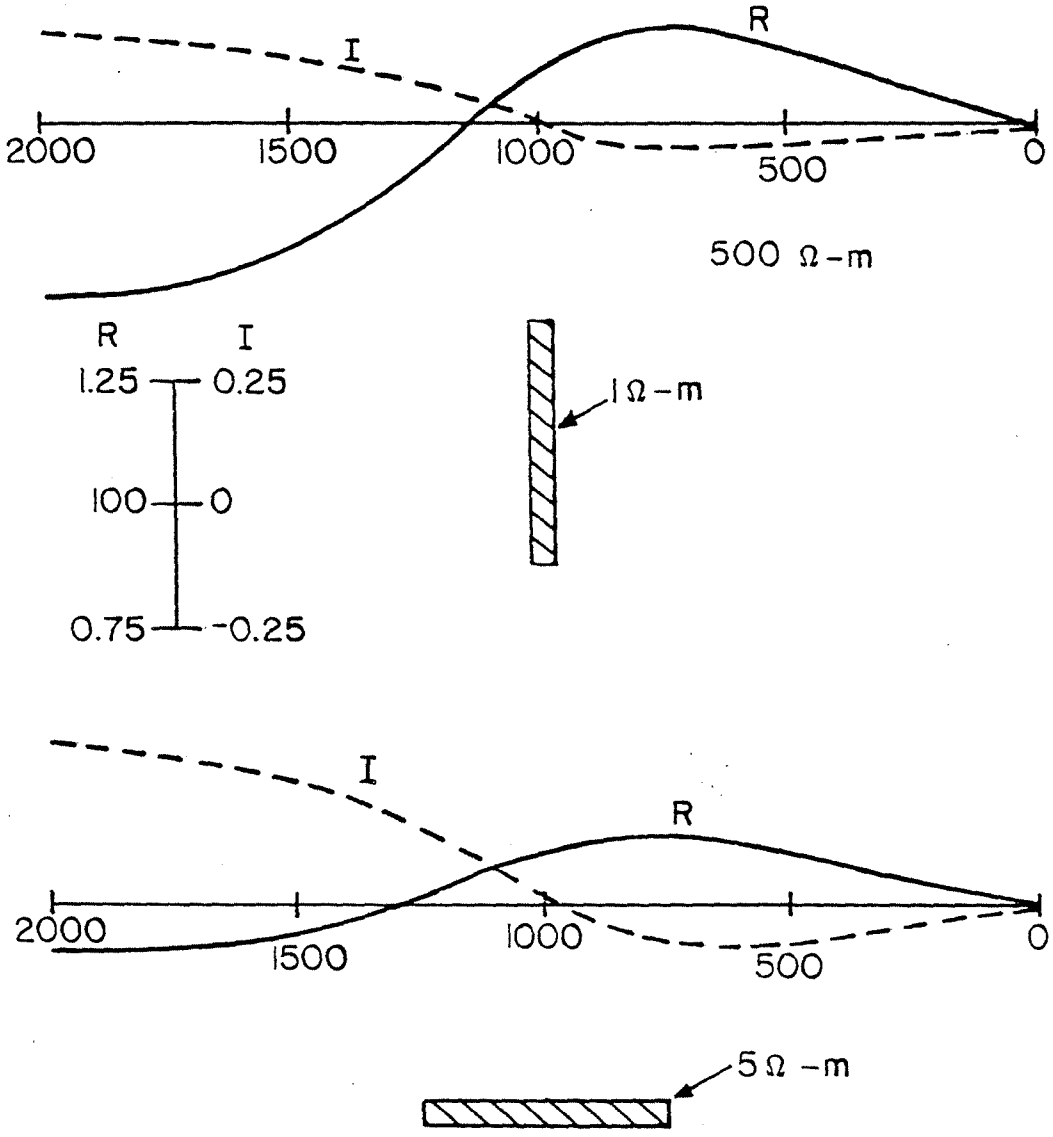
R
I
2000
1500
1000
500
0
500 Ω-m
R
I
1.25
0.25
100
0
0.75
-0.25
1 Ω-m
I
R
2000
1500
1000
500
0
5 Ω-m

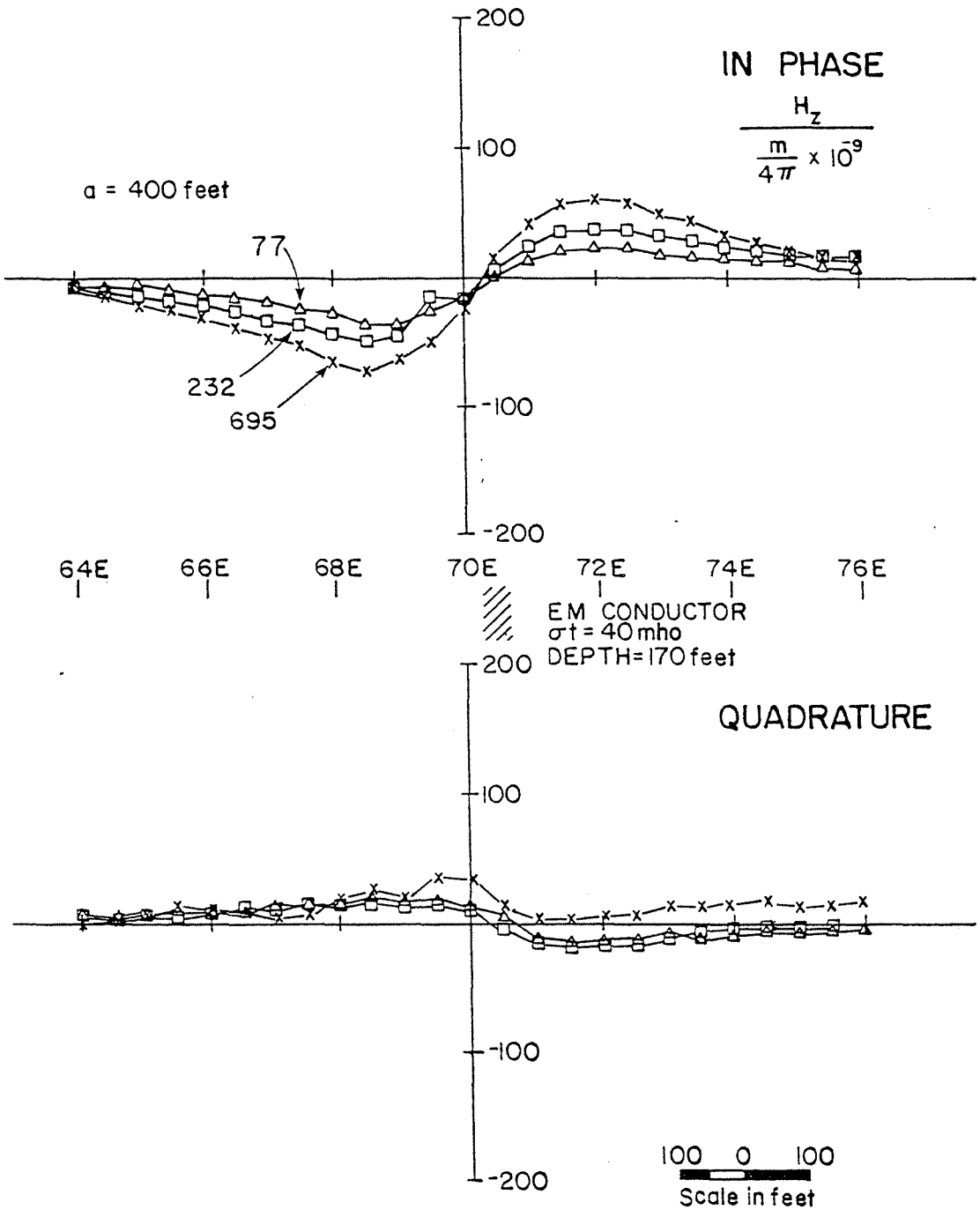
200
IN PHASE
$\frac{H_z}{\frac{m}{4\pi} \times 10^{-9}}$
100
a = 400 feet
77
232
695
-100
-200
64E
66E
68E
70E
72E
74E
76E
EM CONDUCTOR
σt = 40 mho
DEPTH=170 feet
200
QUADRATURE
100
-100
-200
100 0 100
Scale in feet

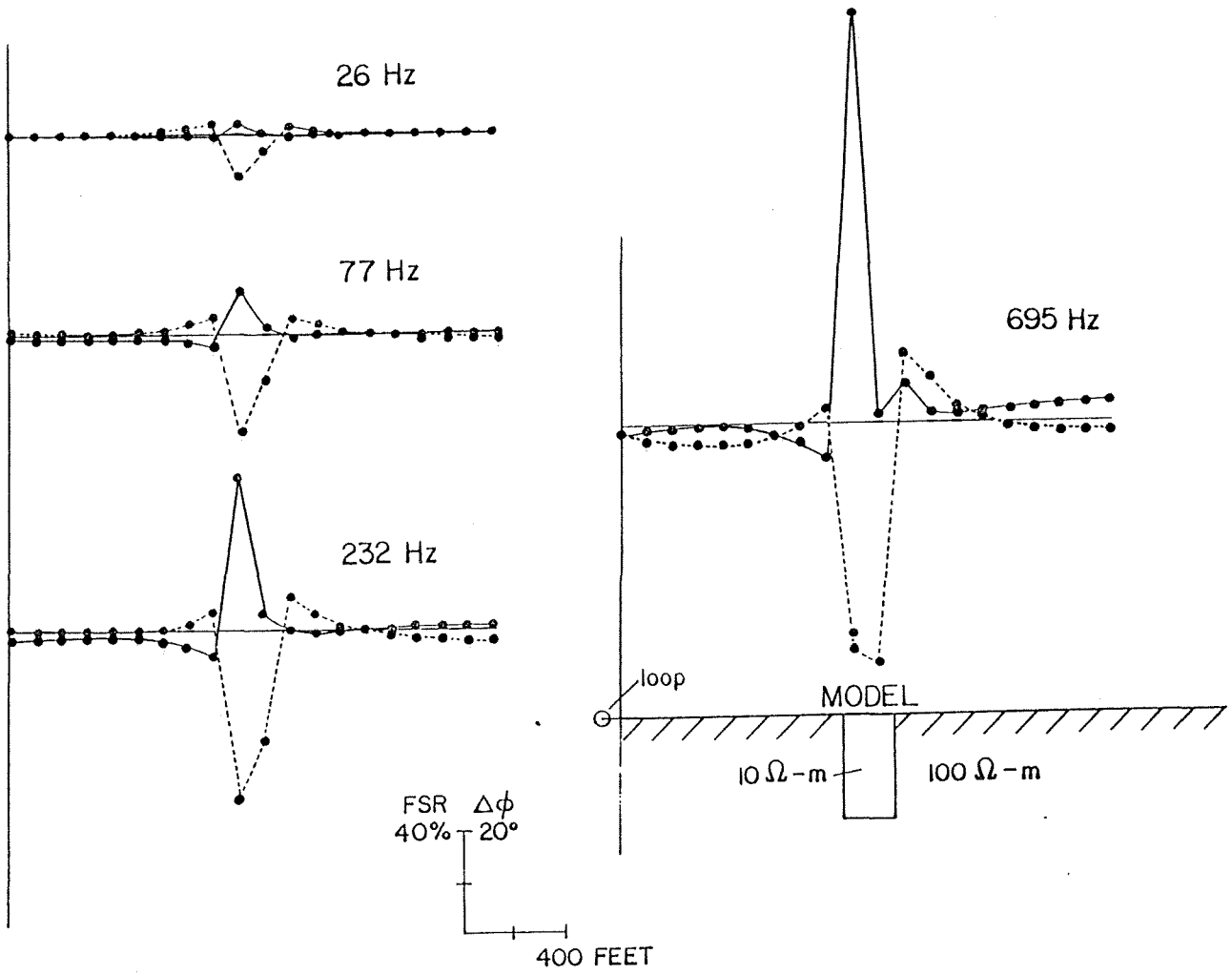
26 Hz
77 Hz
232 Hz
695 Hz
loop
MODEL
10 Ω-m
100 Ω-m
FSR Δϕ
40% 20°
400 FEET

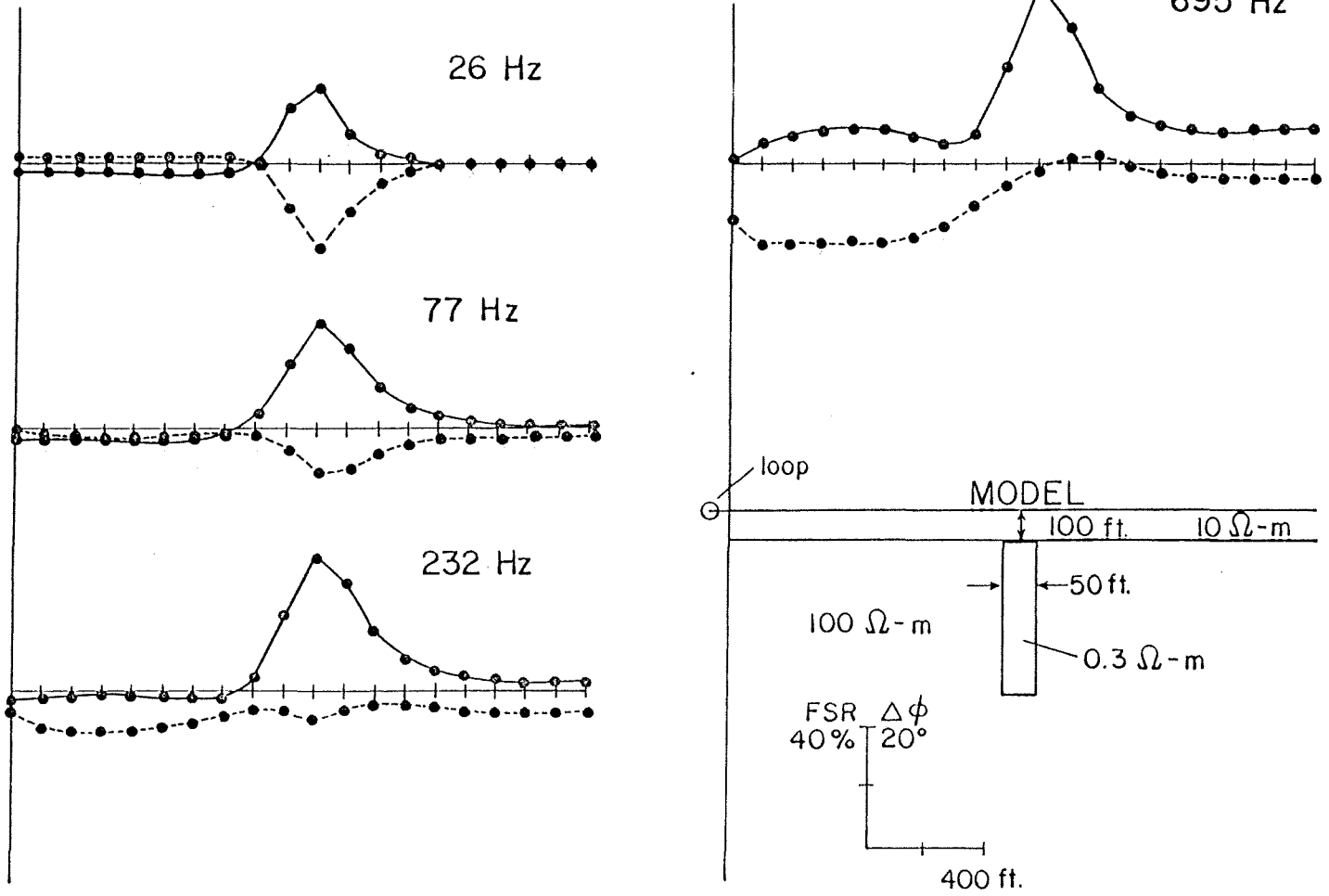
26 Hz
77 Hz
232 Hz
695 Hz
loop
MODEL
100 ft.
10 Ω-m
50 ft.
100 Ω-m
0.3 Ω-m
FSR Δφ
40% 20°
400 ft.

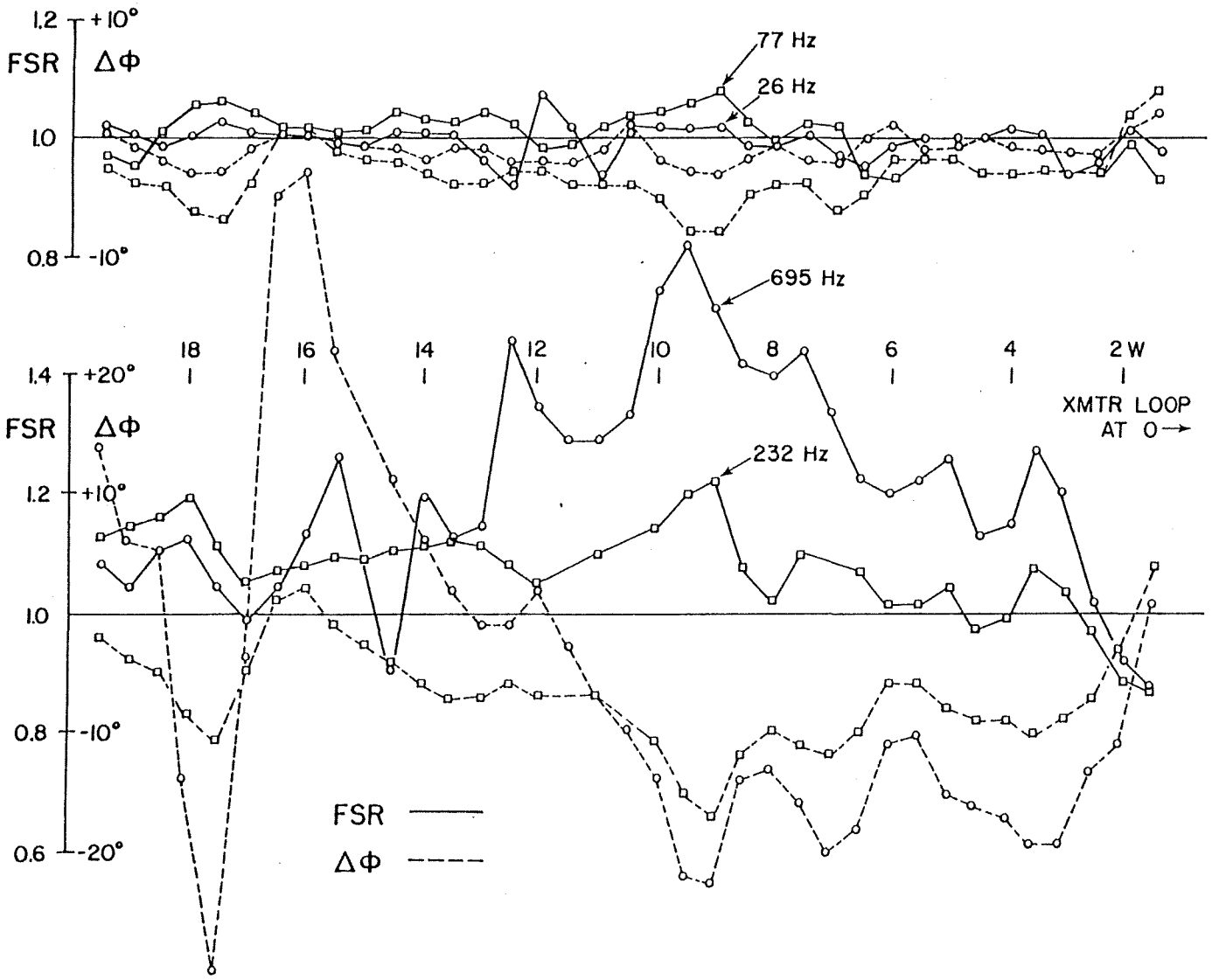
1.2
+10°
FSR
ΔΦ
1.0
0.8
-10°
77 Hz
26 Hz
695 Hz
18
16
14
12
10
8
6
4
2W
XMTR LOOP
AT 0
1.4
+20°
FSR
ΔΦ
232 Hz
1.2
+10°
1.0
0.8
-10°
0.6
-20°
FSR
ΔΦ

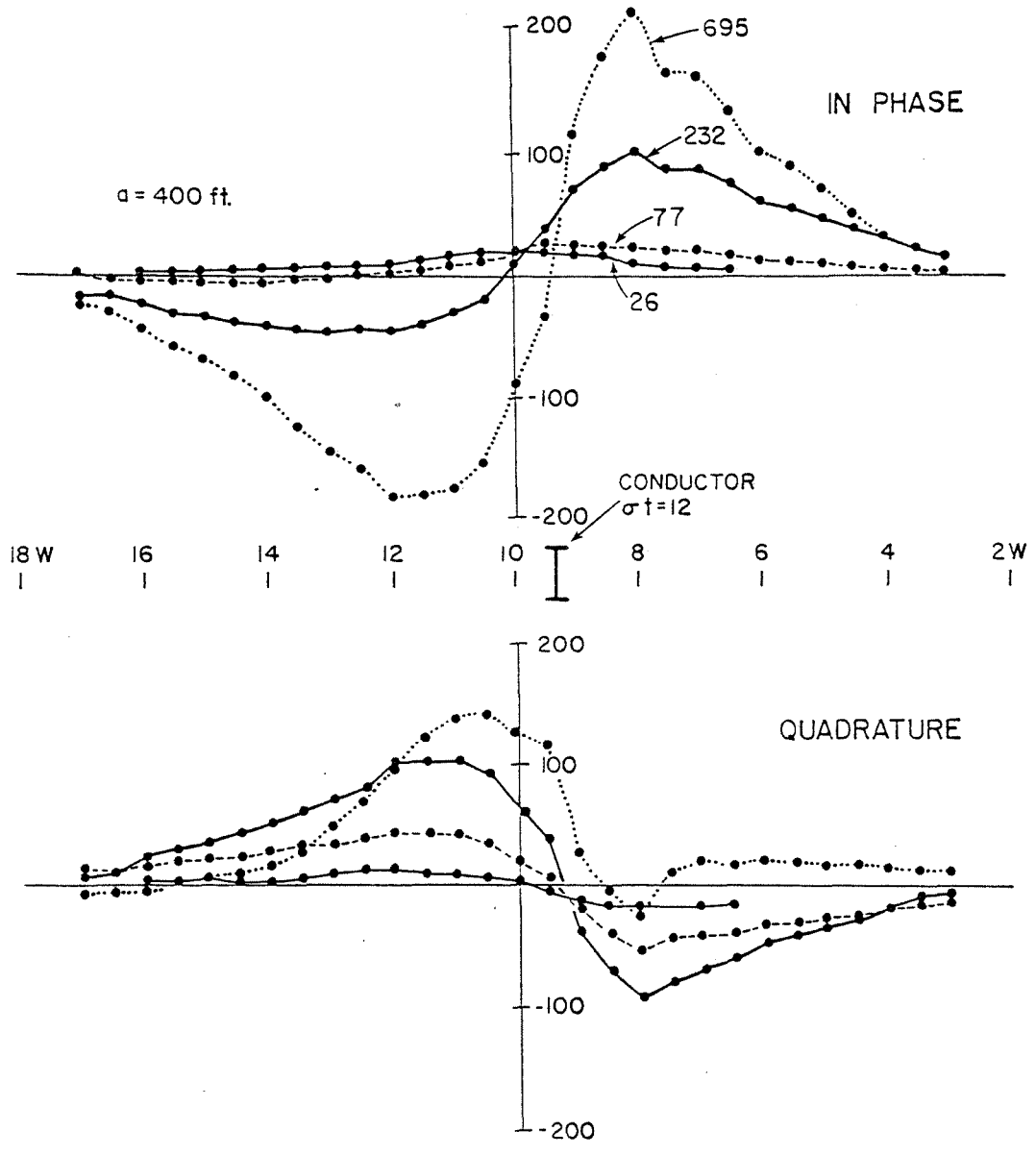
200
695
IN PHASE
100
232
a = 400 ft.
77
26
-100
CONDUCTOR
σt=12
-200
18 W
16
14
12
10
8
6
4
2W
200
QUADRATURE
100
-100
-200

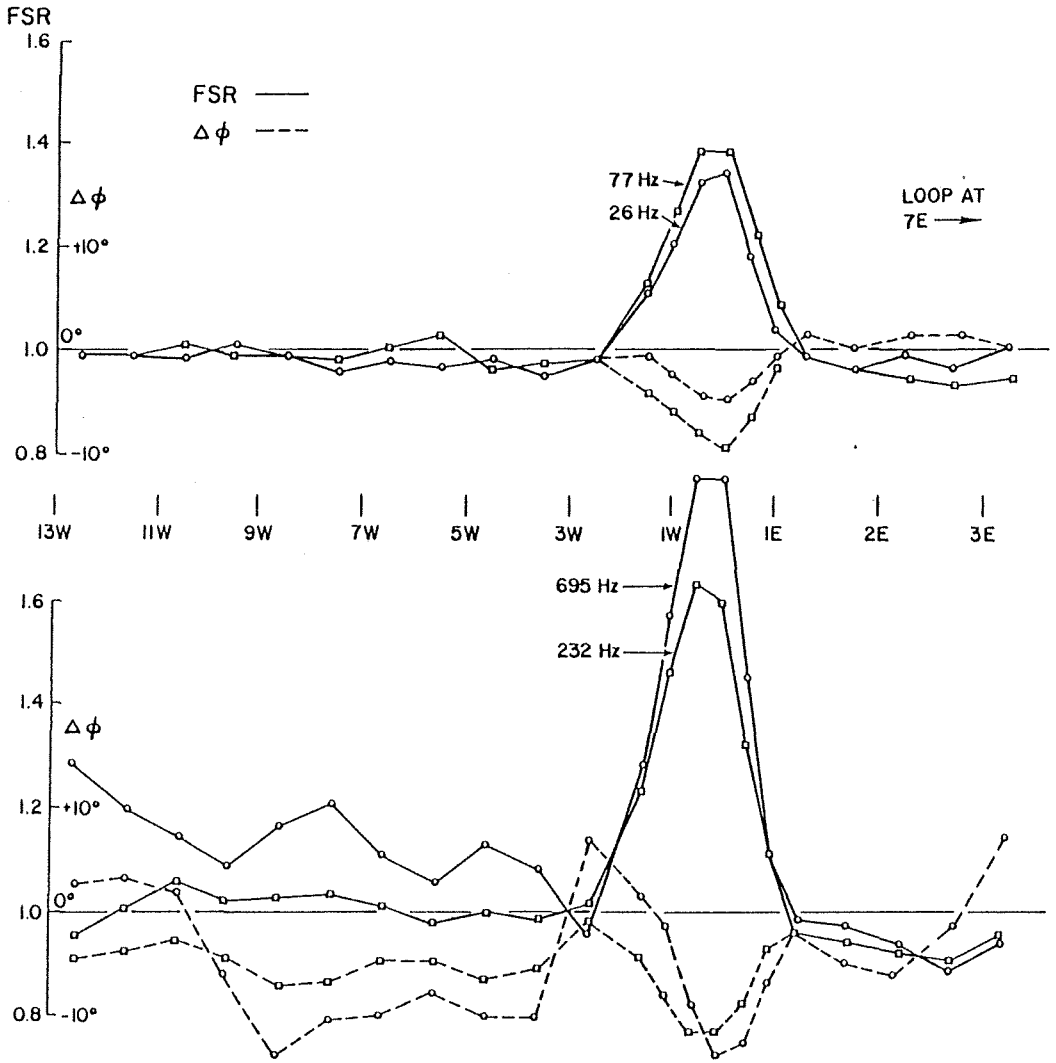
FSR
1.6
1.4
1.2
1.0
0.8
FSR
Δφ
Δφ
+10°
0°
-10°
77 Hz
26 Hz
LOOP AT
7E
13W
11W
9W
7W
5W
3W
1W
1E
2E
3E
695 Hz
232 Hz
1.6
1.4
1.2
1.0
0.8
Δφ
+10°
0°
-10°

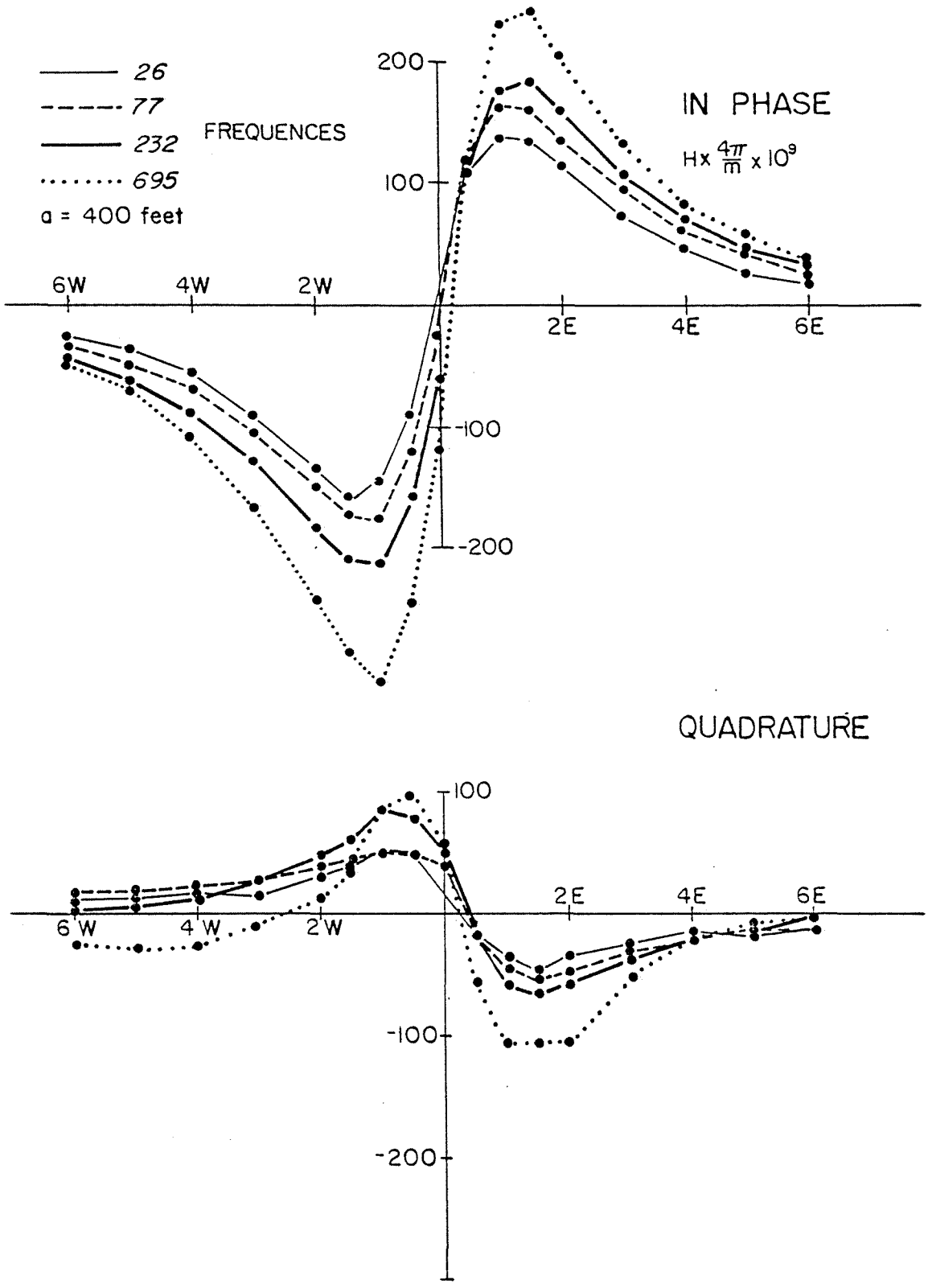
26
77
232
695
a = 400 feet
FREQUENCES
IN PHASE
$H \times \frac{4\pi}{m} \times 10^9$
200
100
-100
-200
6W
4W
2W
2E
4E
6E
QUADRATURE
100
-100
-200
6W
4W
2W
2E
4E
6E

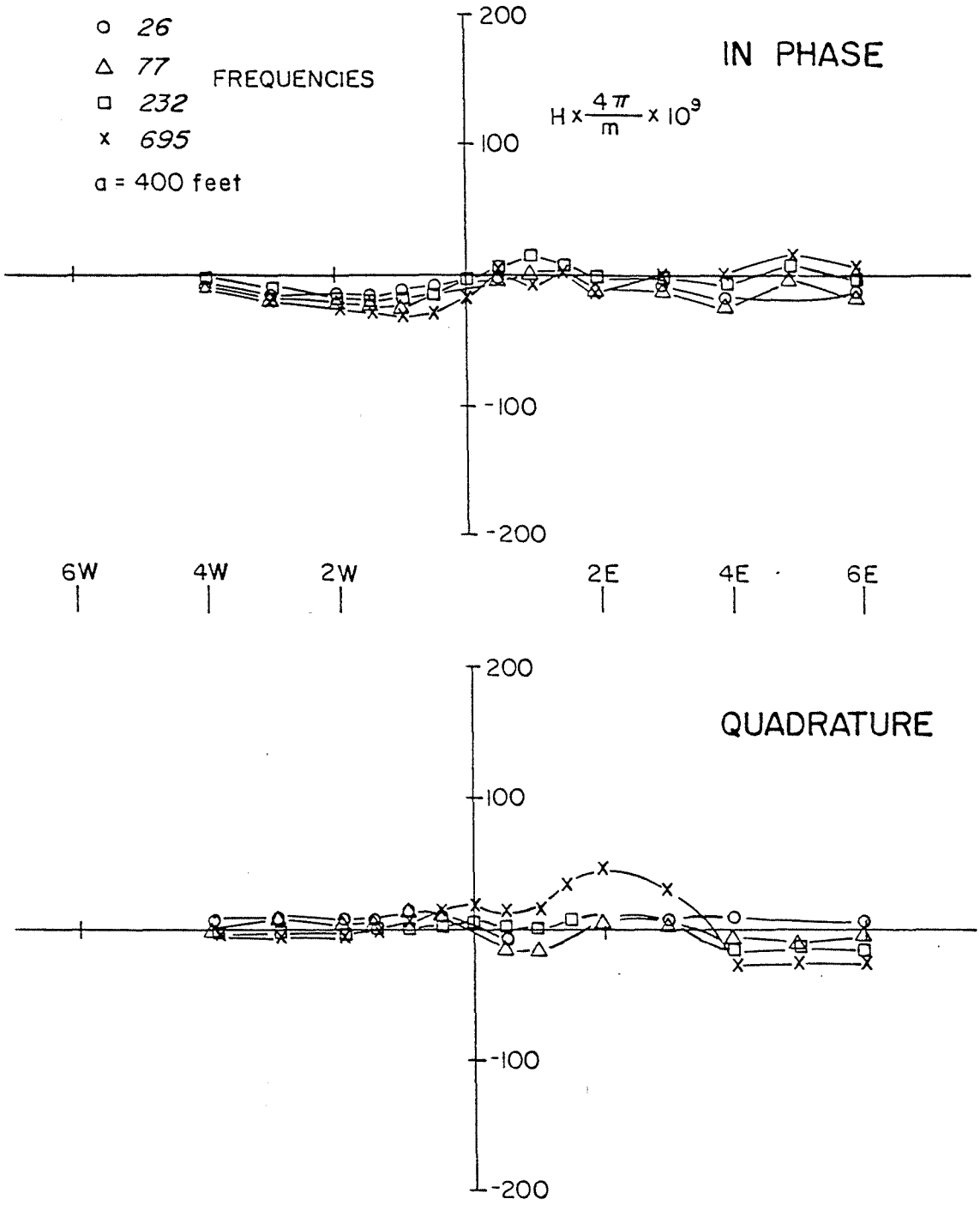
o 26
Δ 77
□ 232
x 695
FREQUENCIES
a = 400 feet
IN PHASE
$H \times \frac{4\pi}{m} \times 10^9$
200
100
-100
-200
6W
4W
2W
2E
4E
6E
QUADRATURE
200
100
-100
-200

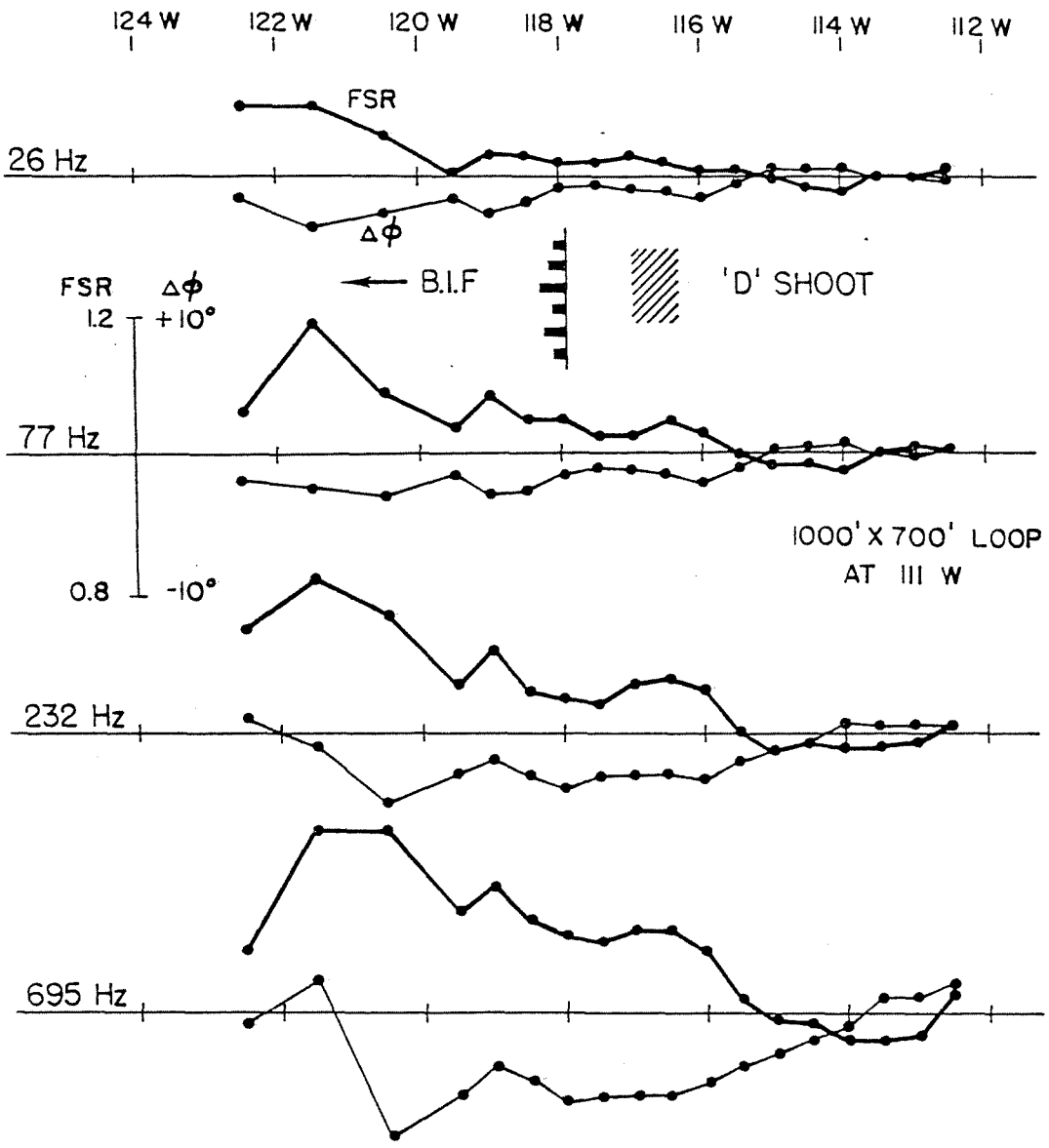
124 W
122 W
120 W
118 W
116 W
114 W
112 W
FSR
26 Hz
Δφ
FSR Δφ
1.2 +10°
B.I.F
'D' SHOOT
77 Hz
1000' X 700' LOOP
AT 111 W
0.8 -10°
232 Hz
695 Hz

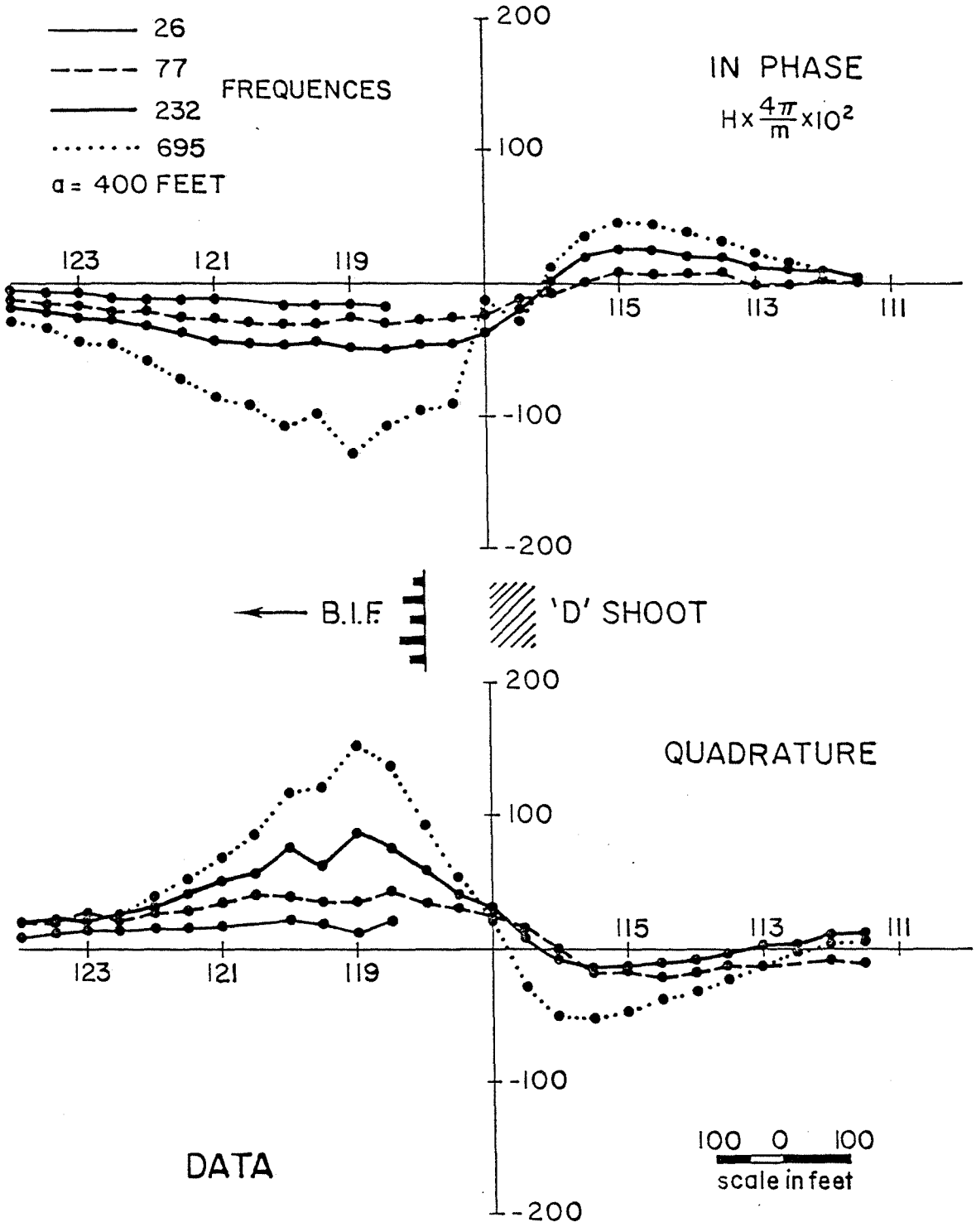
26
77
232
695
FREQUENCES
a = 400 FEET
200
100
-100
-200
IN PHASE
$H \times \frac{4\pi}{m} \times 10^2$
123
121
119
115
113
111
B.I.F.
'D' SHOOT
QUADRATURE
DATA
100 0 100
scale in feet

PLAN VIEW

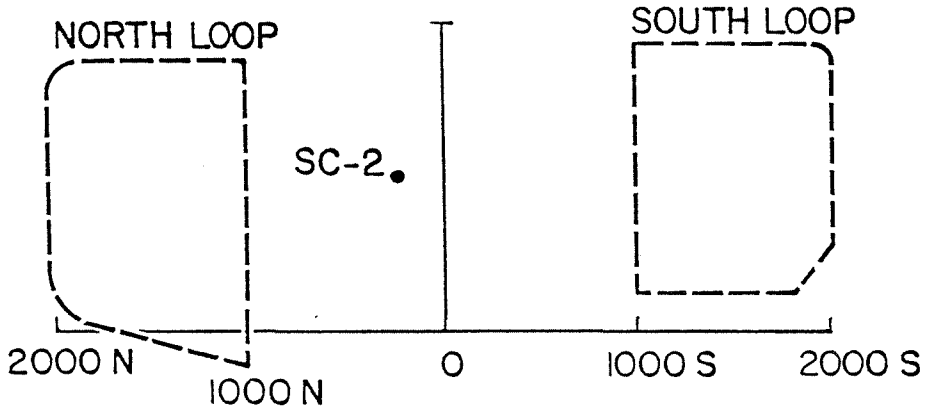

CROSS SECTION

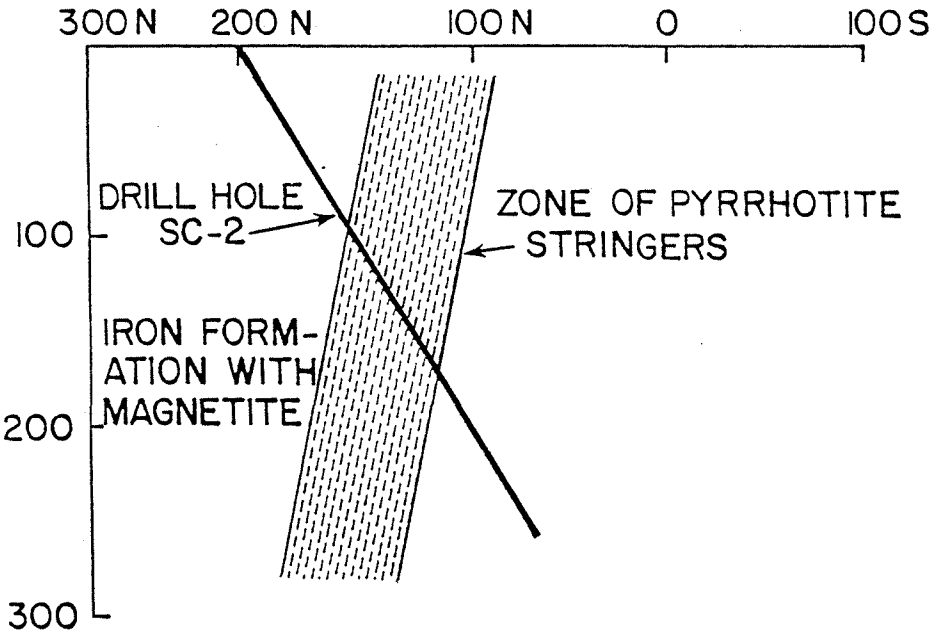

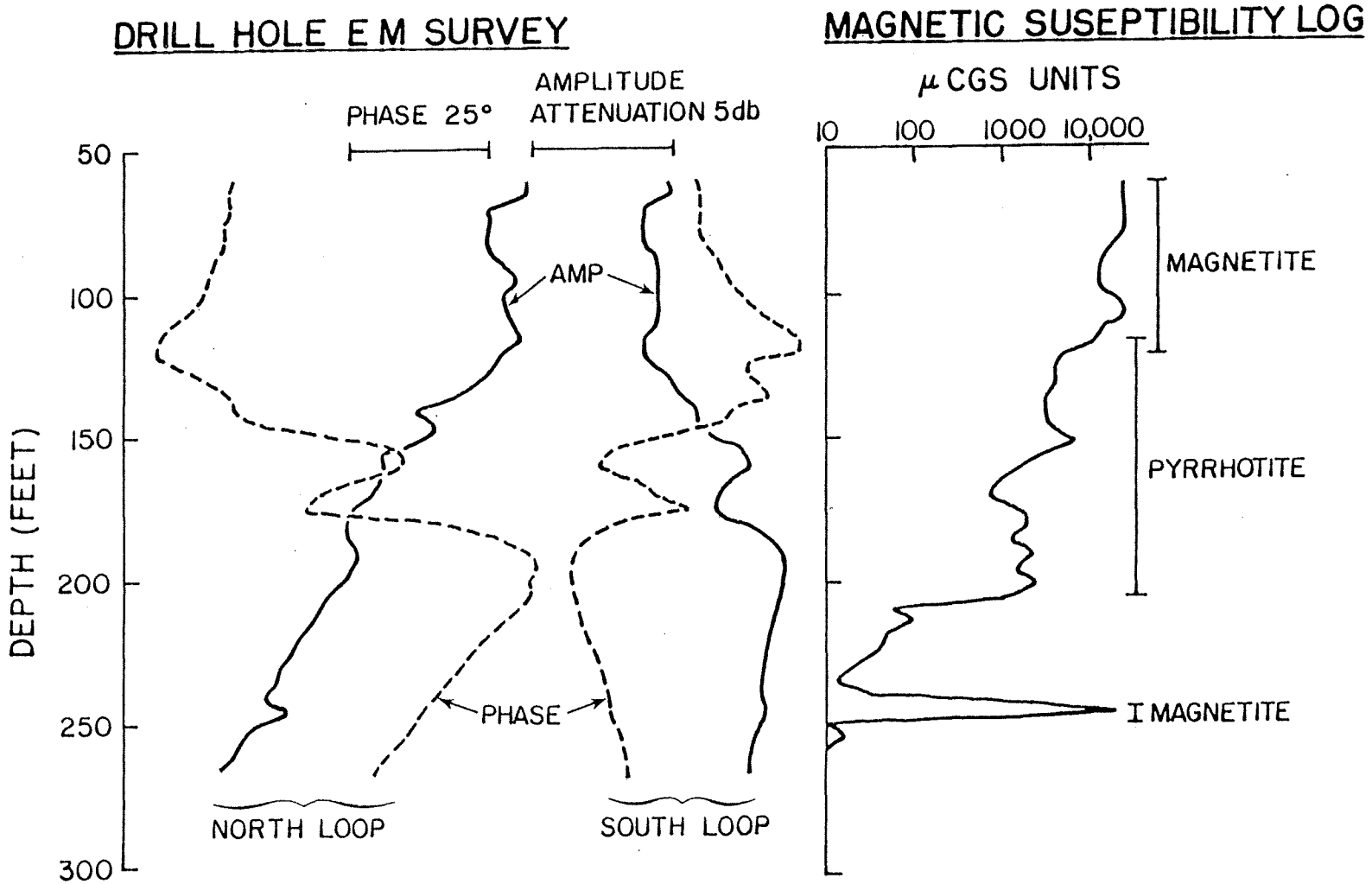
DRILL HOLE E M SURVEY
PHASE 25°
AMPLITUDE ATTENUATION 5db
DEPTH (FEET)
50
100
150
200
250
300
AMP
PHASE
NORTH LOOP
SOUTH LOOP
MAGNETIC SUSEPTIBILITY LOG
μ CGS UNITS
10
100
1000
10,000
MAGNETITE
PYRRHOTITE
I MAGNETITE

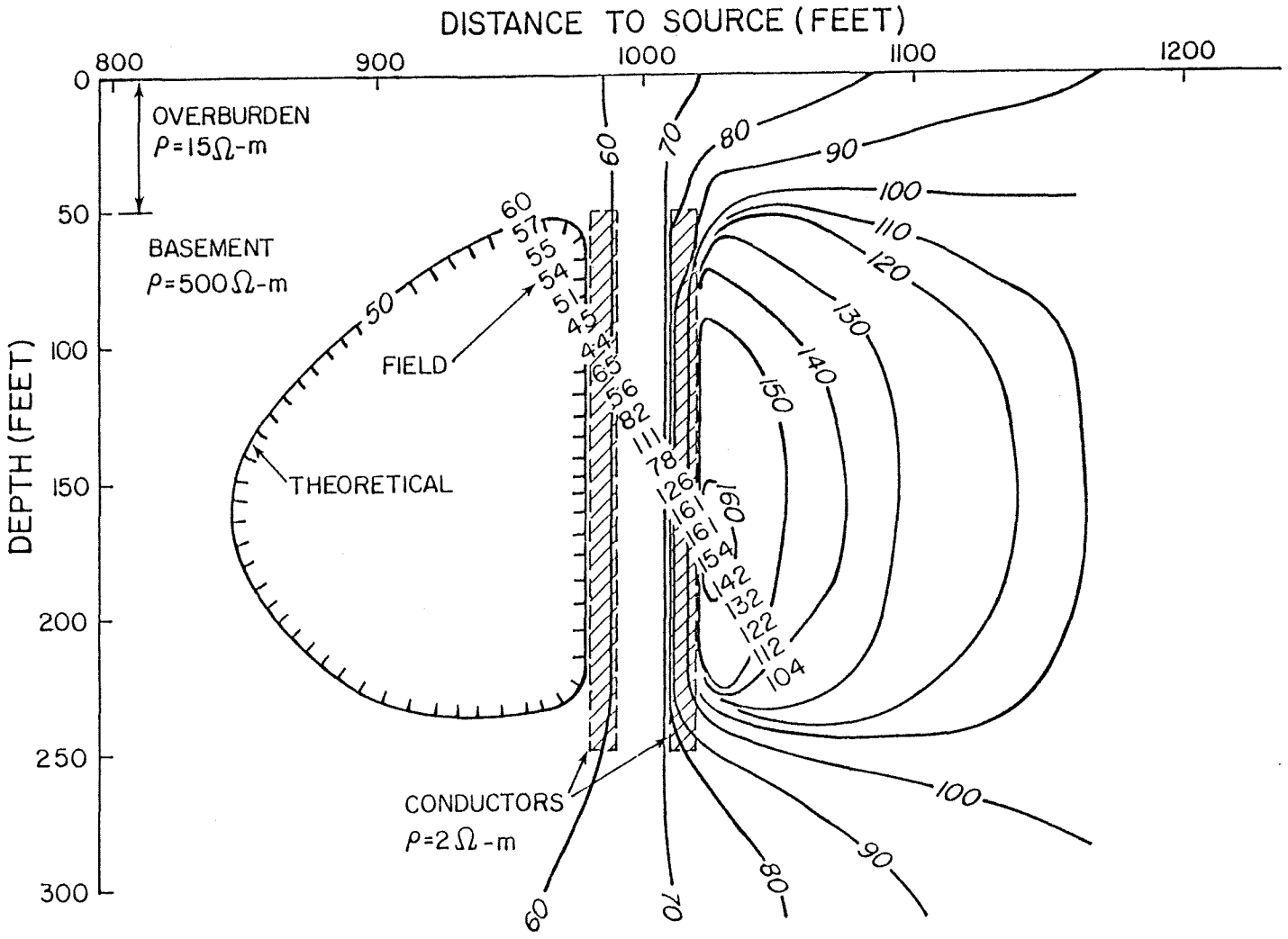
DISTANCE TO SOURCE (FEET)
800
900
1000
1100
1200
0
50
100
150
200
250
300
DEPTH (FEET)
OVERBURDEN
ρ=15Ω-m
BASEMENT
ρ=500Ω-m
FIELD
THEORETICAL
CONDUCTORS
ρ=2Ω-m
60
57
55
54
51
45
44
65
56
82
111
78
126
161
161
154
142
132
122
112
104
60
70
80
90
100
110
120
130
140
150
50
60
70
80
90
100

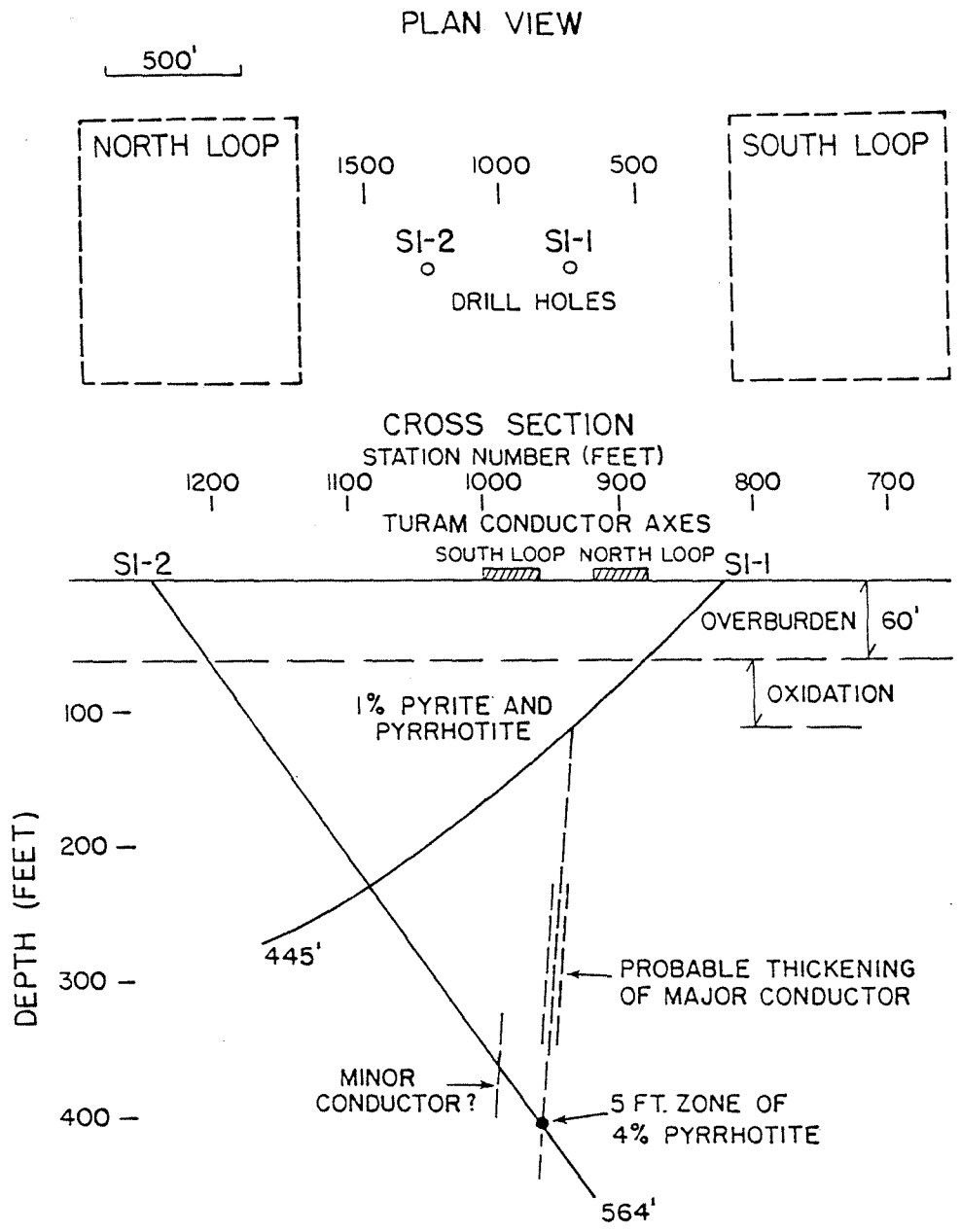
PLAN VIEW
500'
NORTH LOOP
SOUTH LOOP
1500
1000
500
SI-2
SI-1
DRILL HOLES
CROSS SECTION
STATION NUMBER (FEET)
1200
1100
1000
900
800
700
TURAM CONDUCTOR AXES
SOUTH LOOP
NORTH LOOP
SI-2
SI-1
OVERBURDEN
60'
OXIDATION
1% PYRITE AND PYRRHOTITE
DEPTH (FEET)
100
200
300
400
445'
PROBABLE THICKENING OF MAJOR CONDUCTOR
MINOR CONDUCTOR?
5 FT. ZONE OF 4% PYRRHOTITE
564'

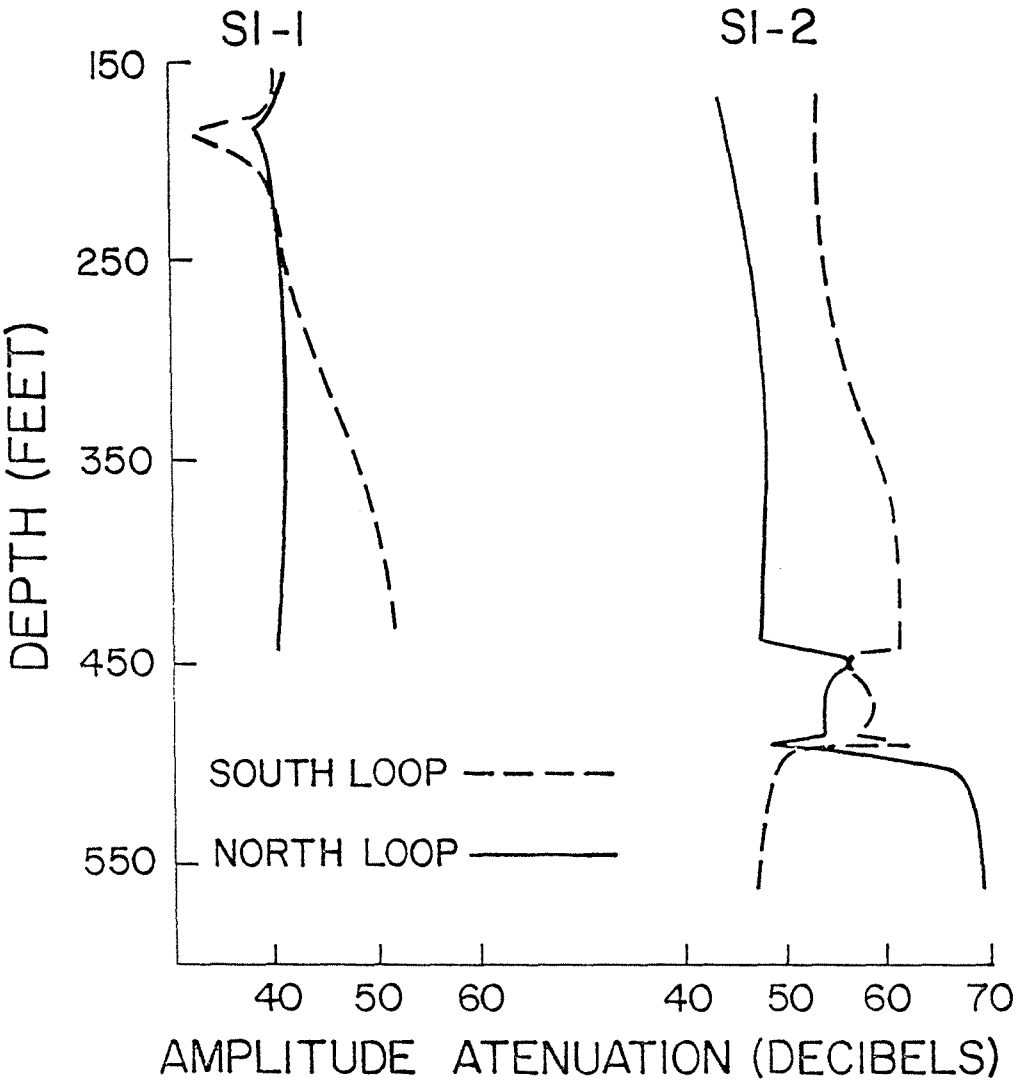
SI-1
SI-2
150
250
350
450
550
DEPTH (FEET)
SOUTH LOOP
NORTH LOOP
40
50
60
40
50
60
70
AMPLITUDE ATENUATION (DECIBELS)

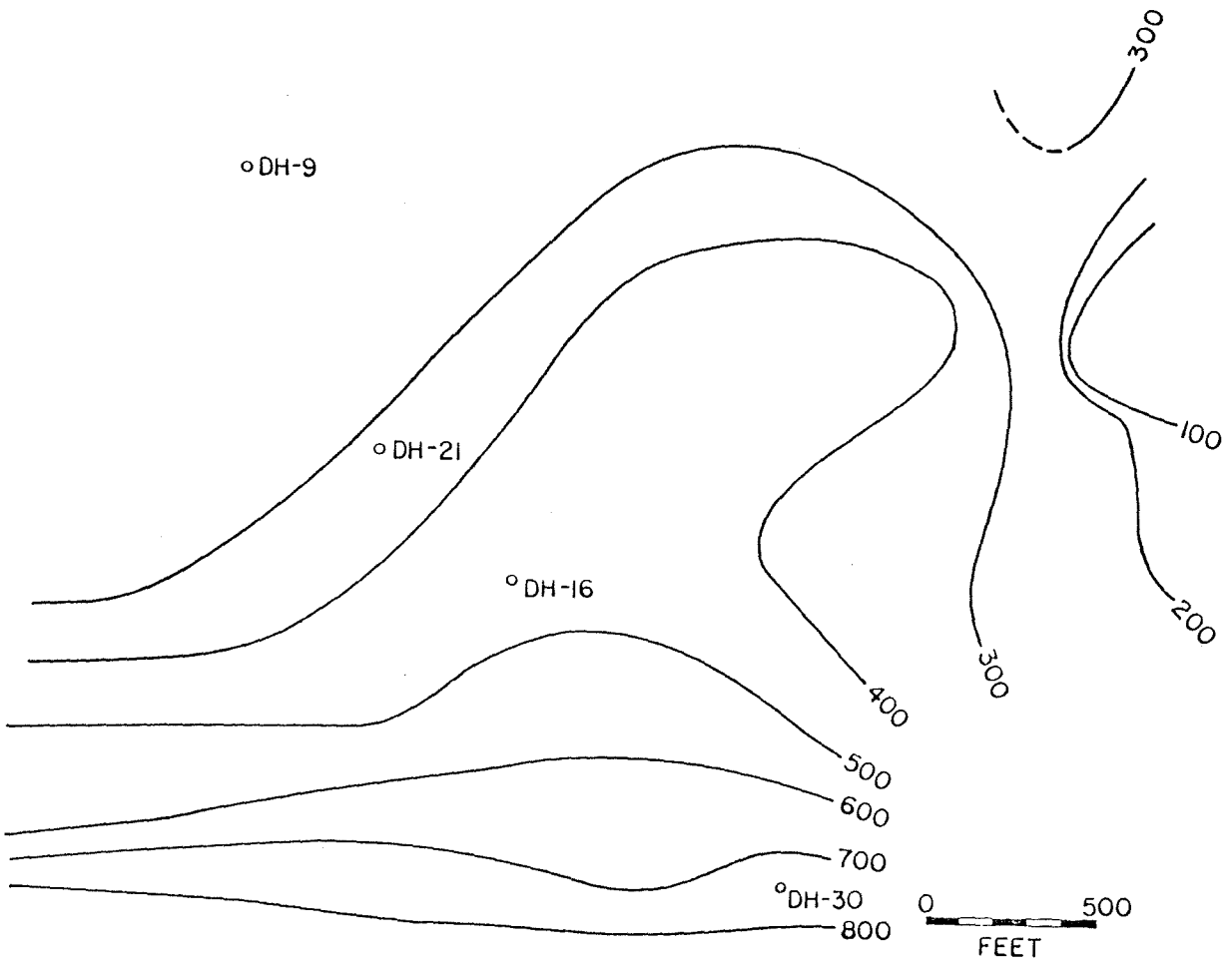
DH-9
DH-21
DH-16
DH-30
300
100
200
300
400
500
600
700
800
0
500
FEET

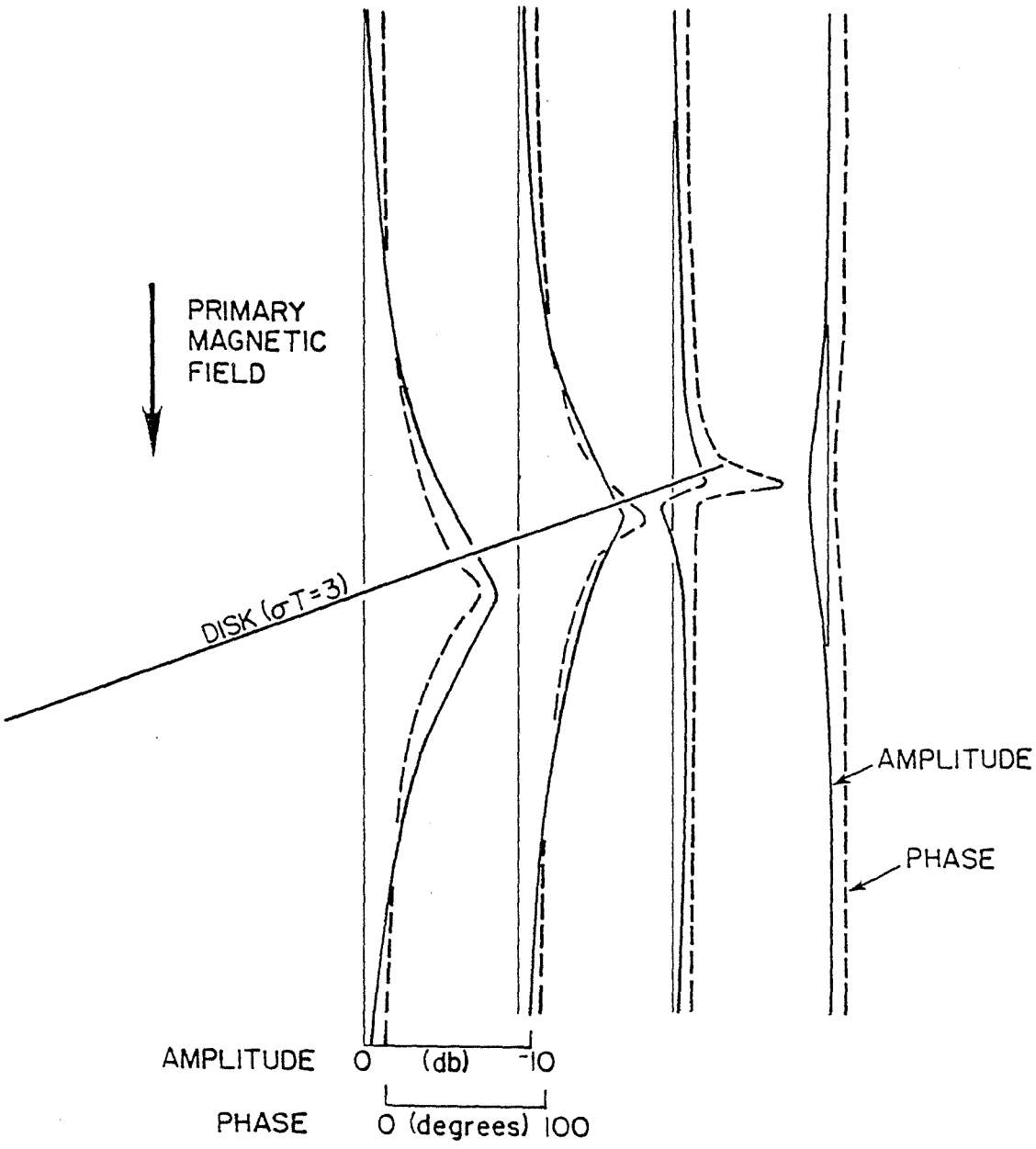
PRIMARY
MAGNETIC
FIELD
DISK (σT=3)
AMPLITUDE
PHASE
AMPLITUDE 0 (db) -10
PHASE 0 (degrees) 100

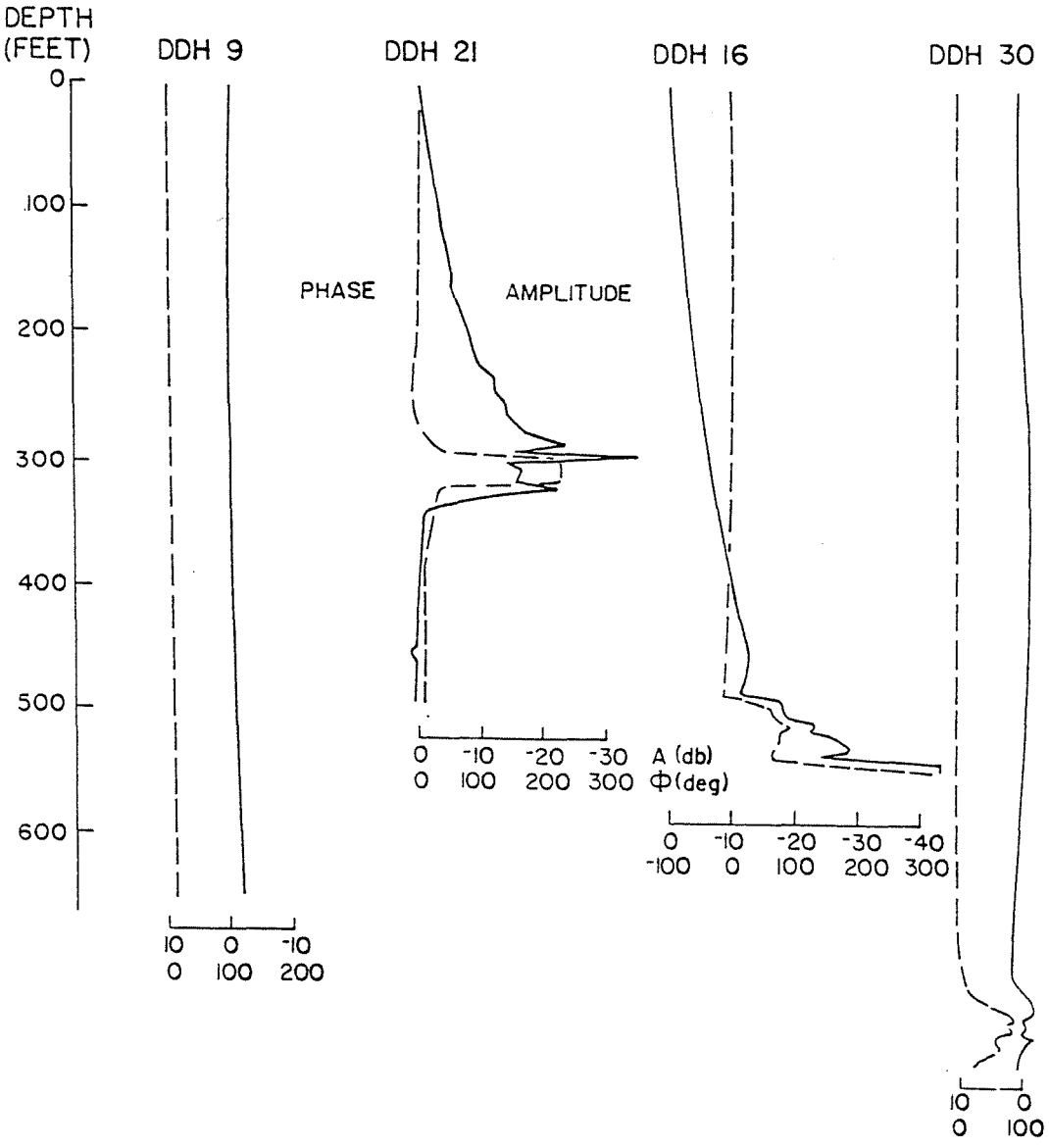
DEPTH
(FEET)
0
100
200
300
400
500
600
DDH 9
10 0 -10
0 100 200
DDH 21
PHASE
AMPLITUDE
0 -10 -20 -30 A (db)
0 100 200 300 Φ(deg)
DDH 16
0 -10 -20 -30 -40
-100 0 100 200 300
DDH 30
10 0
0 100

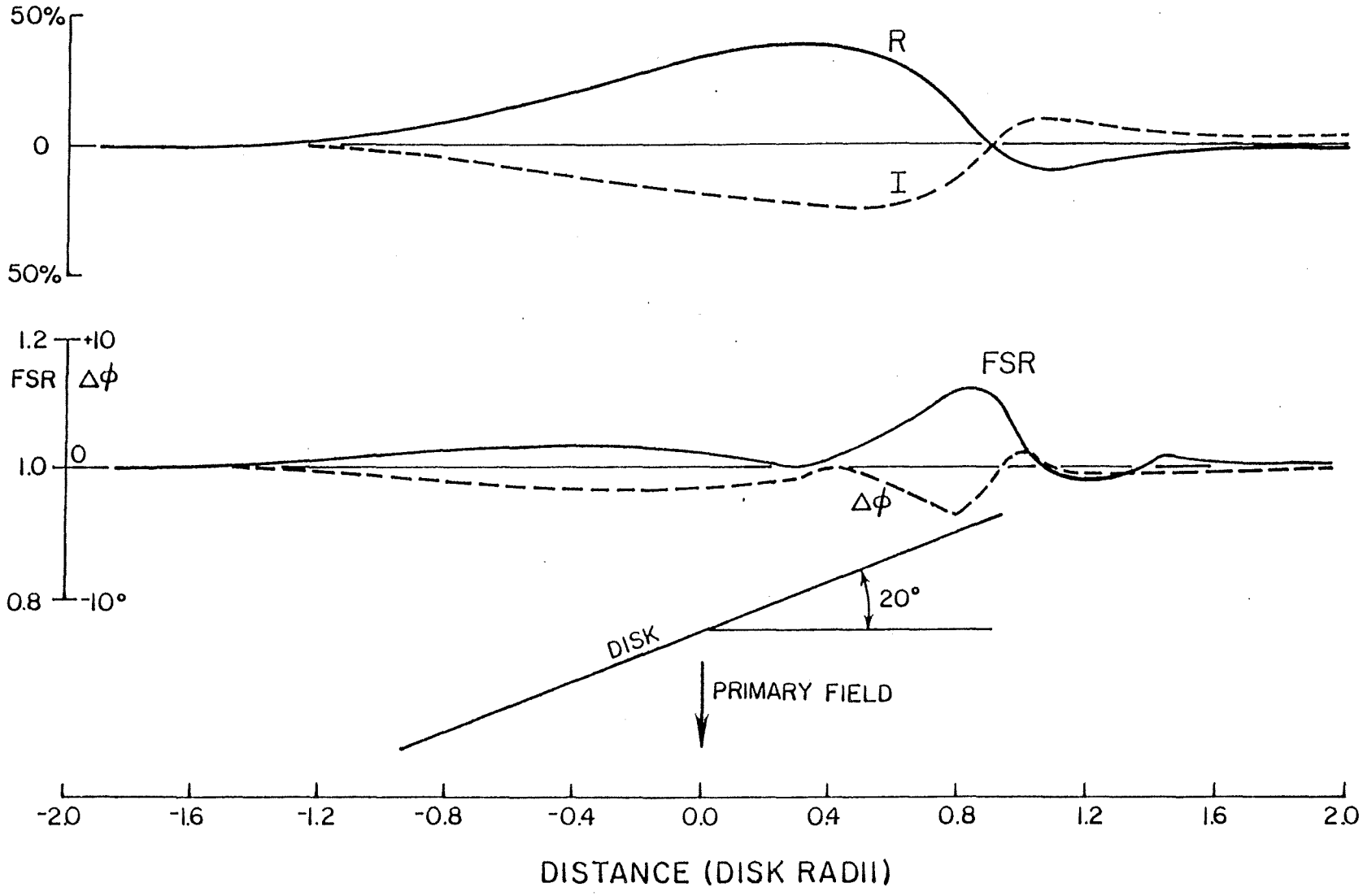
50%
0
50%
R
I
1.2
+10
FSR
Δϕ
1.0
0
0.8
-10°
FSR
Δϕ
20°
DISK
PRIMARY FIELD
-2.0
-1.6
-1.2
-0.8
-0.4
0.0
0.4
0.8
1.2
1.6
2.0
DISTANCE (DISK RADII)

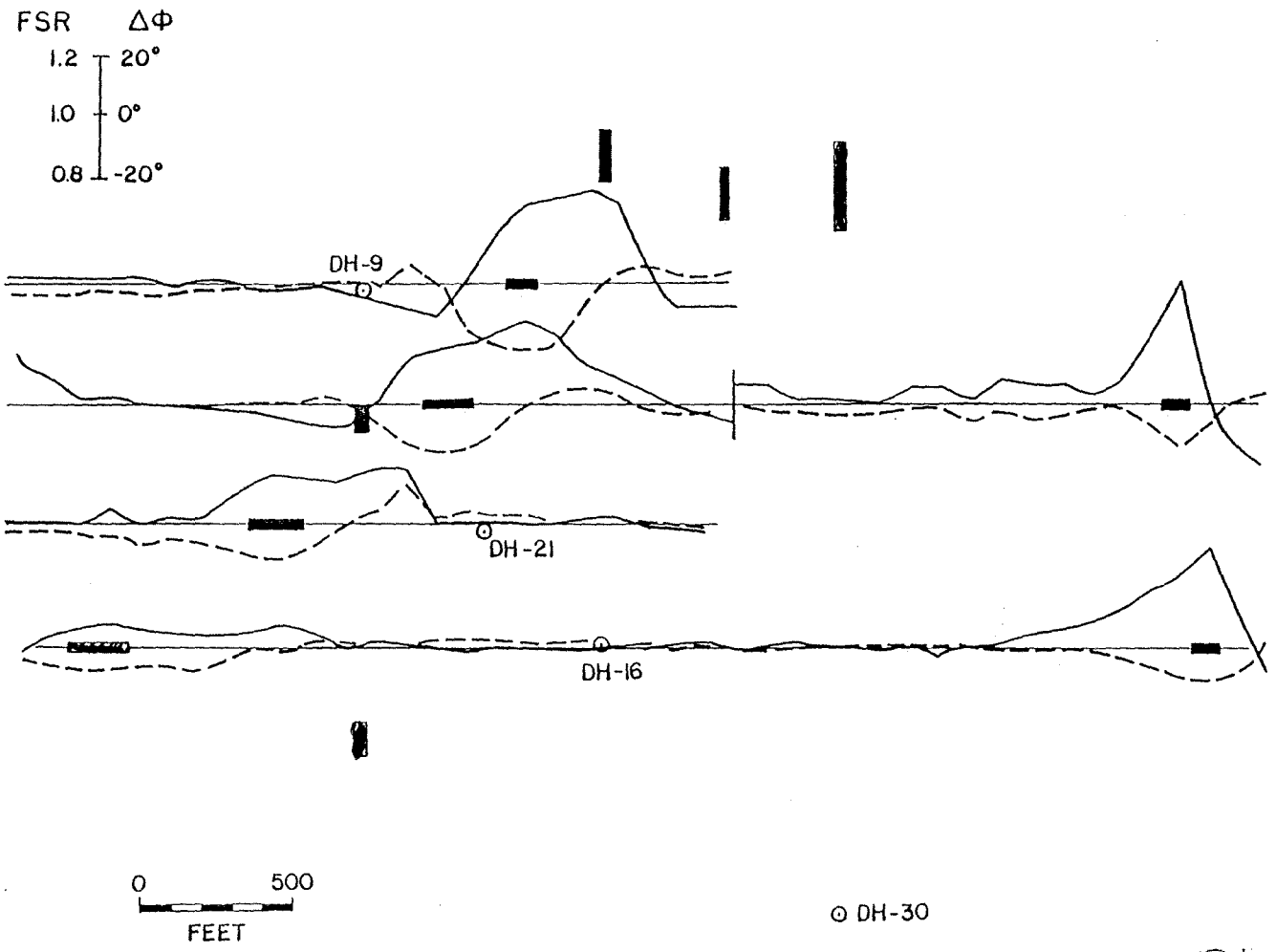
FSR
ΔΦ
1.2
20°
1.0
0°
0.8
-20°
DH-9
DH-21
DH-16
0
500
FEET
⊙ DH-30

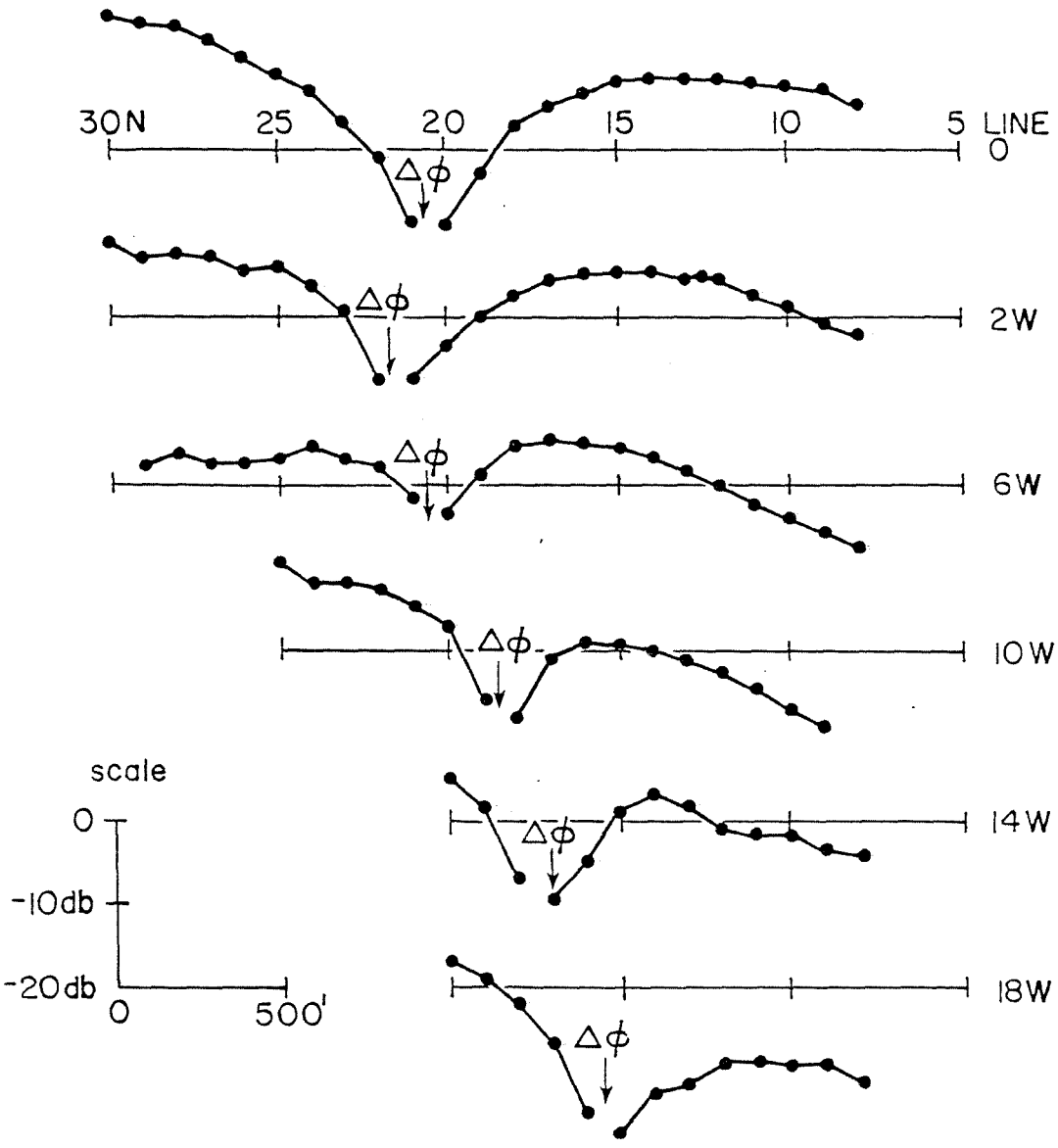
30N
25
20
15
10
5
LINE 0
Δφ
2W
6W
10W
14W
18W
scale
0
-10db
-20db
0
500'

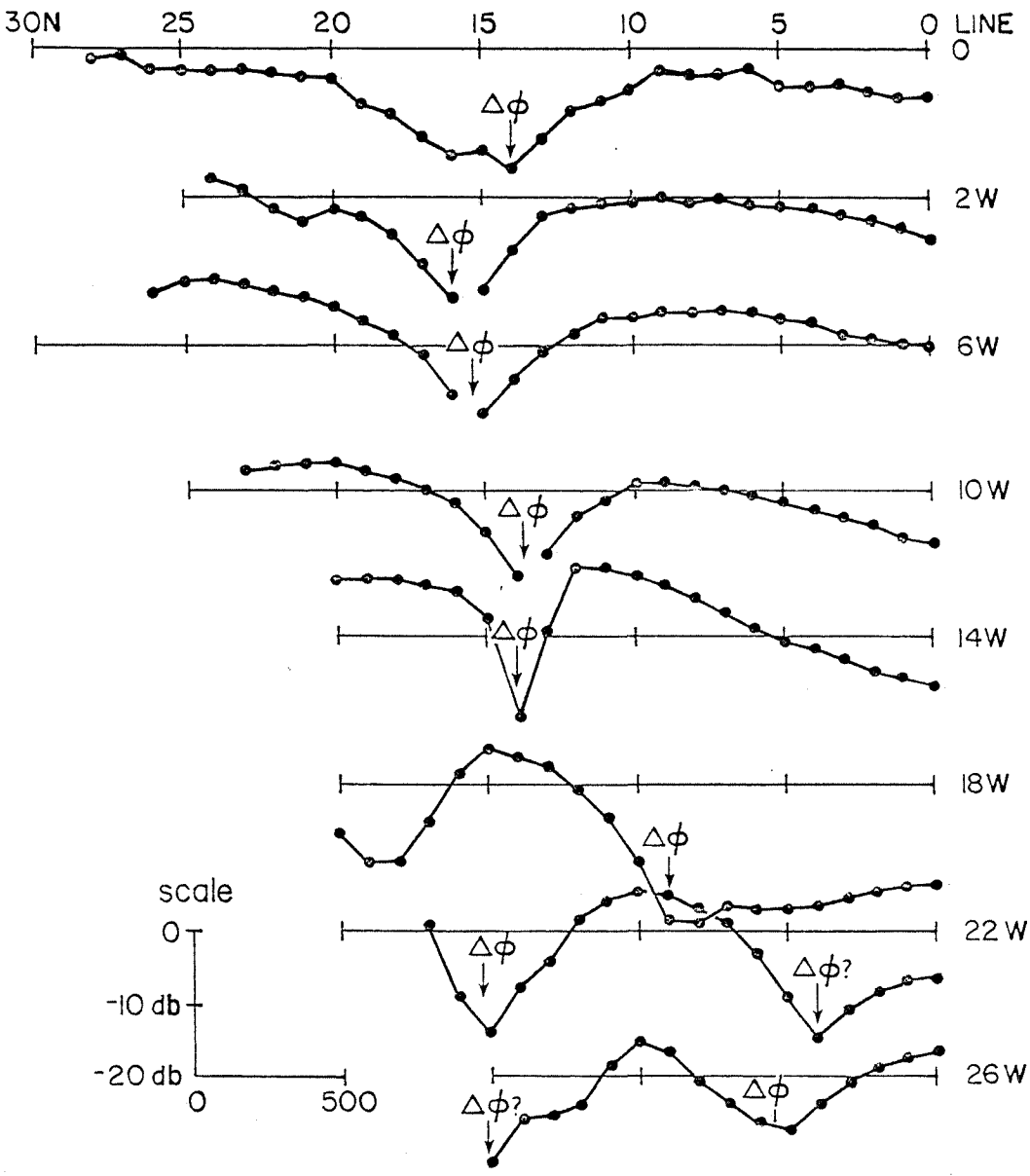
30N
25
20
15
10
5
0 LINE
0
Δφ
2W
Δφ
6W
10W
Δφ
14W
Δφ
18W
Δφ
scale
0
-10 db
-20 db
0
500
Δφ
22W
Δφ?
Δφ?
Δφ
26W

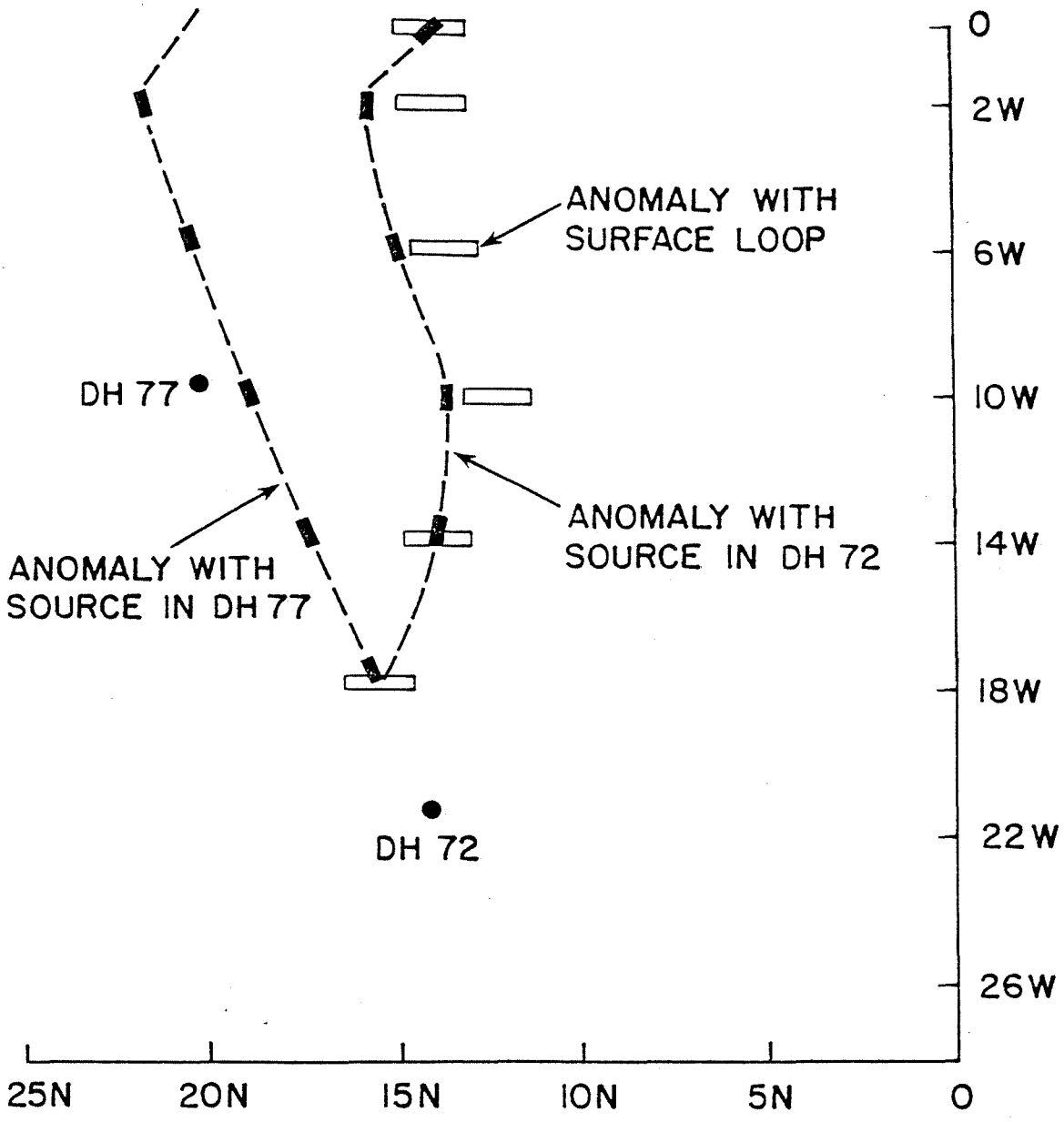
ANOMALY WITH
SURFACE LOOP
DH 77
ANOMALY WITH
SOURCE IN DH 77
ANOMALY WITH
SOURCE IN DH 72
DH 72
0
2W
6W
10W
14W
18W
22W
26W
25N
20N
15N
10N
5N
0